運輸省港湾技術研究所

港湾技術研究所報告

REPORT OF THE PORT AND HARBOUR RESEARCH INSTITUTE

MINISTRY OF TRANSPORT

VOL. 20 NO. 3 SEPT. 1981

NAGASE, YOKOSUKA, JAPAN

港湾技術研究所報告 (REPORT OF P.H.R.I.)
第20巻第3号 (Vol. 20, No. 3), 1981年9月 (Sept. 1981)

目　　次 (CONTENTS)

REPORT OF THE PORT AND
HARBOUR RESEARCH INSTITUTE
Vol. 20 No. 3 (Sept. 1981)

1. Analysis of Edge Waves by Means of Empirical Eigenfunctions

Kazumasa KATOH*

Synopsis

Edge waves, resonant waves trapped in the nearshore by refraction, are characterized by the feature of the surface elevation which varies sinusoidally in the longshore direction and decreases almost exponentially in the offshore direction. The edge waves have recently become of major interest as the cause for the nearshore currents and the surf beats and the formation of the rhythmic toporography. Since the edge waves would not exist indpendently but coexist with incident waves, breaking waves, surf beats, standing waves and nearshore currents, the data measured in the field will contain the effects of all these phenomena. Therefore it is important to separate the components of the edge waves from the field data according to the theories of the edge waves.

This report shows the existence of the standing edge waves by analyzing the longshore variations of wave run-up fronts by means of empirical eigenfunctions. The longshore variations of wave run-up fronts were measured by the aerophotographs at Sendai Beach, Japan, in 1979. At the same time, the waves and the currents were also measured by eight wave staffs and three electromagnetic currentmeters in the surf zone.

The main conclusions of this paper are as follows:

(1) By analyzing the longshore variations of wave run-up fronts by means of the empirical eigenfunctions, the existence of the standing edge waves is demonstrated.

(2) These standing edge waves agree well with those of cutt-off mode predicted by Ball's theory.

(3) An amplitude of the standing edge wave is inversely proportional to its wave number (or frequency).

(4) These standing edge waves are also recognized in cross-spectra of current velocities in the surf zone.

* Senior Research Engineer, Hydraulic Engineering Division

港湾技術研究所報告
第20巻 第3号 (1981. 9)

1. 経験的固有関数によるエッジ波の解析

加 藤 一 正*

要 旨

海浜流，サーフビート，リズミック地形等との関連において，海岸工学における重要性が認識されつつあるエッジ波は，沿岸部にエネルギーがトラップされて生じる波であり，その振幅が汀線位置で最も大きく，沖方向に指数関数的に減少し，水面形状が沿岸方向に周期的に変動するという特徴を有する。エッジ波は，現地において単独で存在することはなく，入射波・砕波・サーフビート・反射定常波・海浜流等と混在している。このため，現地観測データの解析では，これらの諸現象が含まれる測定値のなかから，既応の理論に基づきエッジ波成分を分離することが重要である。

本論文は，1979年に仙台港南海岸で汀線付近の波の遡上線の沿岸方向の変化を測定し，経験的固有関数によって解析することにより，重複エッジ波をとらえたものである。波の遡上線の沿岸方向変化は空中写真から読み取った。また同時に3台の電磁流速計で測定した流速データをクロススペクトル解析することによりそれを確認した。

本論文の主要な結論は以下のとおりである。

1) 波の遡上線の沿岸方向変化を経験的固有関数で解析することにより，複数モードの重複エッジ波が存在していたことが明らかになった。

2) これらの重複エッジ波は，Ball の理論の限界状態のモードに対応している。

3) 各モードの重複エッジ波の振幅はエッジ波の周波数（あるいは波数）に反比例している。

4) 同時に測定した砕波帯内の流れのクロススペクトル解析の結果にも，経験的固有関数で解析されたエッジ波成分が認められた。

* 水工部主任研究官（海浜流解析担当）

Contents

Photo. 1 An aerophotograph of investigated area taken from a balloon lifting at an altitude of around 500 meters. It was just at a low tide on September 19

(a) 14h. 24m. 22s.

(b) 14h. 31m. 22s.

(c) 14h. 50m. 19s.

(d) 15h. 01m. 17s.

Photo. 2 Typical aerophotographs of wave run-up fronts taken from a balloon lifting an altitude of around 500 meters. It was just at a high tide on September 18. In these photographs, it is noticed that the positions of wave run-up fronts on the foreshore vary in the longshore direction. In this paper, the longshore variations of wave run-up fronts are analyzed by means of empirical eigenfunctions in order to detect the standing edge waves.

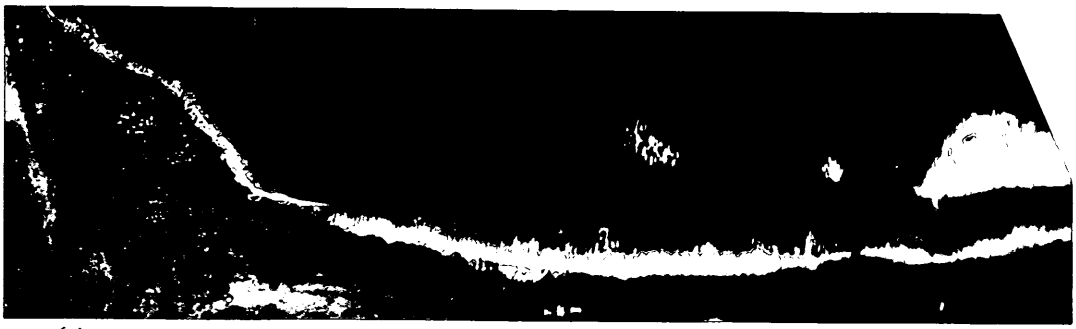

(e) 15h. 10m. 14s.

(f) 15h. 13m. 14s.

(g) 15h. 15m. 14s.

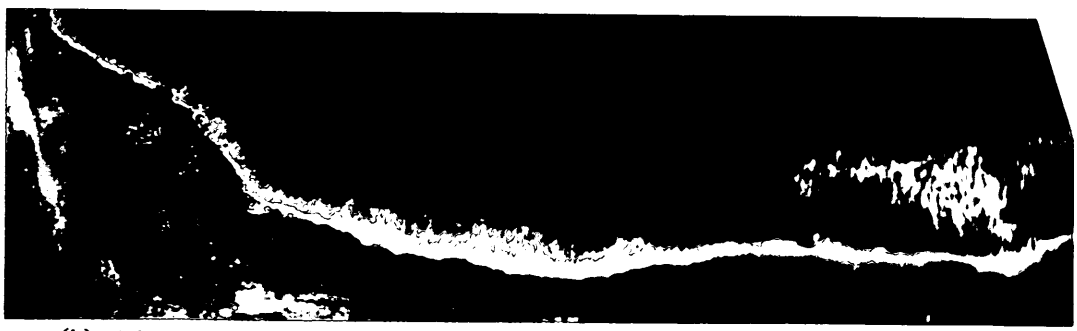

(h) 15h. 17m. 15s.

1. Introduction

Edge waves, resonant waves trapped in the nearshore by refraction, are characterized by the feature of the surface elevation which varies sinusoidally in the longshore direction and decreases almost exponentially in the offshore direction. Generally speaking, the periods and the longshore wavelengths of the edge waves of low mode are about 1–3 minutes and several hundreds meters, respectively. Owing to the order of these scales, the edge waves have recently become of major interest as the cause for the surf beats[1], the generation of the rip currents[2] and the formation of the crescentic bars[3] and beach cusps[4]. But the attempts of investigating the relationships between the edge waves and these phenomena are still hypothetical. And the hypotheses are scarcely examined with the data of field observations.

The history of the theoretical treatments for the edge waves can be traced back to Stokes[5], in 1846, who obtained the solution of the edge wave of zero mode at the beach of constant slope. It was not until about 100 years had passed when this study began to be seriously taken up. Eckart, by means of the shallow water theory, showed that a family of edge wave modes can exist at the beach of constant slope[2]. Ursell[6] solved the small amplitude equations for the edge waves at the beach of constant slope. Ball[7] used the shallow water wave equations to calculate the form of the edge waves at the beach of exponential profile. Guza & Bowen[8] derived the solution of the finite amplitude edge waves to investigate the nonlinear effects. Various features of the edge waves are revealed through these theoretical studies. A feature to be emphasized among them is the existence of a critical frequency, the edge waves with larger frequency than this are trapped in the nearshore zone. This critical frequency is called the cut-off frequency. Ursell[6] suggested that the edge waves of the cut-off frequency might be particularly strongly resonant. Therefore, the discontinuous peaks corresponding to the cut-off frequencies exist in the spectra of the waves in the surf zone. This means that the edge wave of every cut-off frequency is amplified by the mechanism of the frequency selection in the field.

The field observations for the edge waves began in the 1970s, being twenty years behind the theories of Eckart and Ursell. Since the edge waves would not exist independently but coexist with the incident waves, the breaking waves, the surf beats, the standing waves[9], the nearshore currents and so on, the data of the surface fluctuations and currents measured in the field contain the effects of all these phenomena. Therefore it is important to separate the components of the edge waves from the field data according to the theories of the edge waves.

The previous method to separate the edge waves from the field data is to examine, in the light of the edge waves theories, the phase relationship (see

Table 1 Phase relationships between current velocity components (Huntley & Bowen[4])

wave type	u v offshore vs longshore	v w longshore vs vertical	u w offshore vs vertical
progressive gravity	in phase	quadrature	quadrature
standing gravity	quadrature	quadrature	in phase
progressive edge	quadrature	quadrature	in phase
standing edge	in phase	in phase	in phase

Table 1), the coherence and the characteristic of the decay of energy density with the offshore distance, based on the spectral and cross-spectral analyses of the surface fluctuations or the current velocities measured at several points in the surf zone. In this approach, however, the attention is paid only to the one side of the characteristics of the edge waves. Another important side, the water surface varying sinusoidally in the longshore direction, is still remained to be observed in the field.

This report deals with a new observation method of paying attention to the longshore variations of the wave run-up fronts on the foreshore, where the amplitudes of the edge waves are maximum. The results of the empirical eigenfunction analysis[10),11)] for the longshore variations of wave run-up fronts show the existence of the standing edge waves near the large breakwater prolonged normal to the shore. The previous method is also used to analyze the current velocities measured simultaneously in the surf zone for comfirming the existence of the standing edge waves.

2. Theory of edge waves and examples measured in the field

2.1 Theory of edge waves

Since the edge waves of low mode are the long period waves in the near-shore zone, these waves can be considered to be shallow water waves. The basic equations of shallow water waves are the equation of motion,

$$\frac{\partial u}{\partial t}+g\frac{\partial \zeta}{\partial x}=0, \tag{1}$$

$$\frac{\partial v}{\partial t}+g\frac{\partial \zeta}{\partial y}=0, \tag{2}$$

and that of continuity,

$$\frac{\partial \zeta}{\partial t}+\frac{\partial}{\partial x}(hu)+\frac{\partial}{\partial y}(hv)=0, \tag{3}$$

where x is the coordinate perpendicular to the shoreline, increasing offshore from zero at the shoreline, y is the coordinate parallel to the shoreline and u and v are the velocity components in the offshore and the longshore directions. And ζ is the displacement of the free surface from the static equilibrium position, h is the water depth and g is the acceleration of gravity. In order

to simplify the theoretical treatments, we assume that the shoreline is a strait line and the beach profile is uniform in the longshore direction, depending only on x.

Based on these assumptions, Eckart and Ball gave the theoretical solutions of the edge waves on a beach of constant slope and on a beach of exponential profile, respectively[2),7)]. Here Ball's theory is shown.

The beach of exponential profile of the form

$$h=h_0[1-\exp(-\alpha x)], \tag{4}$$

was selected by Ball. As the water surface configuration of the edge wave is sinusoidal in the longshore direction, we put

$$\zeta(x,y,t)=A(x)\cos(ky-\sigma t), \tag{5}$$

for the edge wave propagating in the positive longshore direction, where k is the longshore wave number and σ is the angular frequency. Integrating Eq. (1) and Eq. (2) with respect to t by substituting Eq. (5) into these equations, we have

$$u=\frac{g}{\sigma}\sin(ky-\sigma t)\frac{dA(x)}{dx}, \tag{6}$$

$$v=\frac{gk}{\sigma}\cos(ky-\sigma t)A(x). \tag{7}$$

By using Eqs. (5), (6) and (7), Eq. (3) reduces to

$$\sigma A(x)+h\left\{\frac{g}{\sigma}\frac{d^2A(x)}{dx^2}-\frac{gk^2}{\sigma}A(x)\right\}+\frac{g}{\sigma}\frac{dA(x)}{dx}\frac{dh}{dx}=0. \tag{8}$$

Here we put

$$\left.\begin{aligned} &S=\exp(-\alpha x),\\ &h=h_0(1-S),\\ &G(S)=A(x),\end{aligned}\right\} \tag{9}$$

then

$$\left.\begin{aligned} &\frac{dh}{dx}=\alpha h_0 S,\\ &\frac{dA(x)}{dx}=-\alpha S\frac{dG(S)}{dS},\\ &\frac{d^2A(x)}{dx^2}=\alpha^2 S\frac{dG(S)}{dS}+\alpha^2S^2\frac{d^2G(S)}{dS^2}.\end{aligned}\right\} \tag{10}$$

By substituting Eq. (10) into Eq. (8), we have

$$(1-S)S^2\frac{d^2G(S)}{dS^2}+(1-2S)S\frac{dG(S)}{dS}+[\omega^2-(1-S)m^2]G(S)=0, \tag{11}$$

where $\omega^2=\sigma^2/gh_0\alpha^2$ and $m^2=k^2/\sigma^2$. We also put $G(S)=S^pF(S)$, then

$$\left.\begin{aligned} &\frac{dG}{dS}=pS^{p-1}F(S)+S^p\frac{dF(S)}{dS},\\ &\frac{d^2G}{dS^2}=p(p-1)S^{p-2}F(S)+2pS^{p-1}\frac{dF(S)}{dS}+S^p\frac{d^2F(S)}{dS^2}.\end{aligned}\right\} \tag{12}$$

By using Eq. (12), Eq. (11) reduces to

$$S^{p+2}(1-S)\frac{d^2F}{dS^2}+S^{p+1}\{1+2p-2(p+1)S\}\frac{dF}{dS}$$
$$+S^p\{S(m^2-p^2-p)+p^2+\omega^2-m^2\}F=0. \tag{13}$$

If we put

$$p^2+\omega^2-m^2=0, \tag{14}$$

and divide Eq. (13) by S^{p+1}, we have ultimately

$$S(1-S)\frac{d^2F}{dS^2}+\{1+2p-2(p+1)S\}\frac{dF}{dS}-(p+p^2-m^2)F=0. \tag{15}$$

Equation (15) is the Gaussian differential equation, the solution of which is provided by

$$F=F(\alpha,\beta;\gamma:S)=1+\sum_{k=1}^{\infty}\frac{\alpha(\alpha+1)\cdots(\alpha+k-1)\beta(\beta+1)\cdots(\beta+k-1)}{k!\gamma(\gamma+1)\cdots(\gamma+k-1)}S^k \tag{16}$$

and

$$\left.\begin{aligned}&\alpha+\beta+1=2p+2\\&\alpha\beta=p^2+p-m^2\\&\gamma=1+2p,\end{aligned}\right\} \tag{17}$$

where $F(\alpha,\beta;\gamma:S)$ is the hypergeometric function. Ball derived the finite series expression of Eq. (16) by putting

$$\alpha=-n, \tag{18}$$

where n is a positive integer. Then the equations of

$$\beta=2p+1+n \tag{19}$$

and

$$m^2=(p+n)(p+n+1), \tag{20}$$

are valid.

The summary of the theory for the progressive edge wave is;

$$\zeta(x,y,t)=A(x)\cos(k_ny-\sigma_nt), \tag{21}$$
$$A(x)=a_n\exp(-p\alpha x)\cdot F(-n,n+2p+1;2p+1:\exp(-\alpha x)), \tag{22}$$
$$p^2=\left(\frac{k_n}{\alpha}\right)^2-\sigma_n^2/gk_0\alpha^2 \quad \text{(from Eq. 14)} \tag{23}$$

and

$$\left(\frac{k_n}{\alpha}\right)^2=(p+n)(p+n+1) \quad \text{(from Eq. 20)}, \tag{24}$$

where n is the modal number of the edge wave, a_n is the shoreline amplitude, k_n is the longshore wave number corresponding to the edge wave of n-th mode, respectively. A pair of Eqs. (23) and (24) is the dispersion relation with a connecting parameter p. **Figure 1** shows the dispersion curves predicted by Eqs. (23) and (24); the exponential parameter α and k_0 are so chosen to fit the beach profile at Sendai Beach, Japan (see **Fig. 7** and Eq. 40).

For the standing edge wave, Eqs. (5), (6) and (7) are replaced by

$$\zeta(x,y,t)=A(x)\sin k_ny\cdot\sin\sigma_nt, \tag{25}$$
$$u=\frac{g}{\sigma_n}\sin k_ny\cdot\cos\sigma_nt\cdot\frac{dA(x)}{dx} \tag{26}$$

and

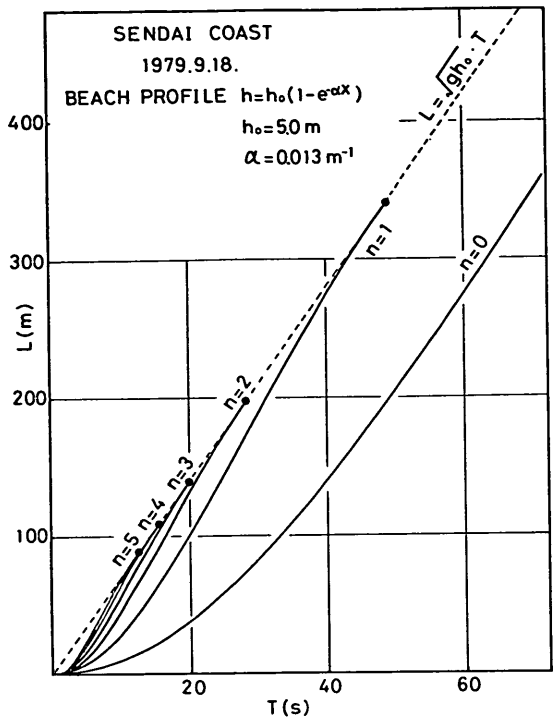

Fig. 1 Dispersion curves of edge waves predicted by Ball's theory

$$v=\frac{gk_n}{\sigma_n}\cos k_n y\cdot\cos\sigma_n t\cdot A(x). \tag{27}$$

The expressions for $A(x)$, k_n and σ_n for the standing edge wave are the same with Eqs. (22), (23) and (24).

Ball's solution shows a nearly similar tendency as Eckart's one. An interesting feature of Ball's theory, however, is the prediction of the cut-off periods, the edge wave with longer periods than this being nontrapped and radiating energy away from the nearshore zone. According to Eq. (22), the cut-off mode corresponds to $p=0$, then Eqs. (23) and (24) reduce to

$$k_n=\alpha\sqrt{n(n+1)} \quad \text{(cut-off wave number)}, \tag{28}$$

$$\sigma_n=\alpha\sqrt{n(n+1)gk_0} \quad \text{(cut-off angular frequency)}. \tag{29}$$

Equations (28) and (29) show that the cut-off wave number depends only on α and the cut-off frequency depends on both α and k_0. The dispersion relation of the cut-off mode agrees with that of the shallow water waves on the horizontal sea bed. Equations (28) and (29) are valid for $n\geqq 1$, but the cut-off mode for $n=0$ will be predicted if the Corioli's force will be taken into account.

The hypergeometric functions with $p=0$ for the first seven mode are

$$n=1\text{: } F=1-2S, \tag{30}$$

$$n=2\text{: } F=1-6S+6S^2, \tag{31}$$

$$n=3:\ F=1-12S+30S^2-20S^3, \tag{32}$$

$$n=4:\ F=1-20S+90S^2-140S^3+70S^4, \tag{33}$$

$$n=5:\ F=1-30S+210S^2-560S^3+630S^4-252S^5, \tag{34}$$

$$n=6:\ F=1-42S+420S^2-1680S^3+3150S^4-2772S^5+924S^6, \tag{35}$$

$$n=7:\ F=1-56S+756S^2-4200S^3+11550S^4-16632S^5 +12012S^6-3432S^7, \tag{36}$$

where $S=\exp(-\alpha x)$. These equations show that the water surface profiles of the edge waves in the offshore direction depend only on α. Since the longshore wavelength of edge waves also depend only on α, as previously mentioned, ultimately the water surface profiles both in the longshore and the offshore directions depend on the exponential parameter α.

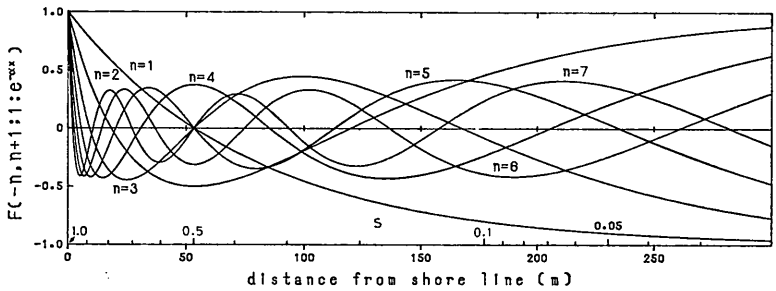

Fig. 2 Hypergeometric functions for the first seven cut-off mode

The hypergeometric functions of the cut-off mode ($p=0$) are shown in Fig. 2 by adjusting the value of each F being positive at the shoreline ($S=1$). The distance from the shoreline with $\alpha=0.013$ is also shown on the horizontal axis. We can observe in this figure the following features of the edge waves. The amplitude is maximum at the shoreline ($S=1$) and decreases with the distance from the shoreline. But it gradually increases again and recovers the value at the shoreline as the distance further increases. The modal number gives a number of zero crossings of the edge wave profile of each mode. The location of $S=0.5$ corresponds to a node of the edge wave of every odd mode and a anti-node of the edge wave of every even mode.

Figure 3 shows the three dimensional profile of the standing edge wave of $n=2$ mode. The nodal lines which are kept in the same positions are represented with thick solid lines.

The phase relationship between u and v is in quadrature ($\pi/2$ or $3\pi/2$) for the progressive edge waves according to Eqs. (6) and (7), while it is in phase (0 or π) for the standing ones according to Eqs. (26) and (27). Depending on this difference of phase relationship between the standing and the progressive edge waves, whether the edge waves are the standing or the progressive ones is determined by the cross-spectral analysis between u and v components.

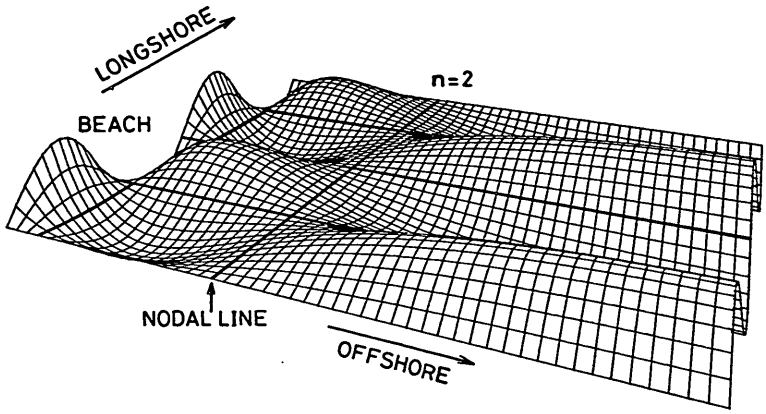

Fig. 3 Three dimensional water surface profile of standing edge wave of $n=2$ mode

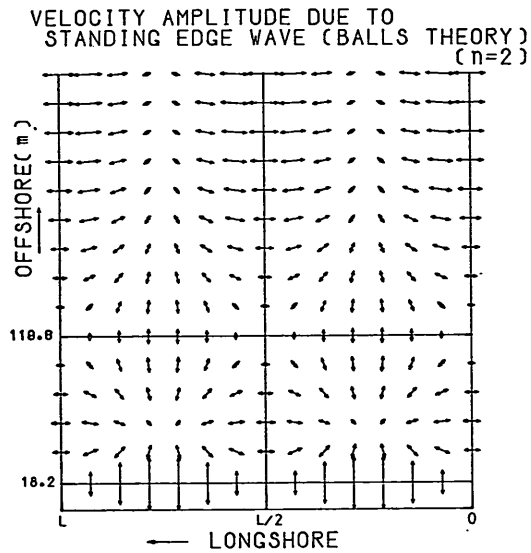

Fig. 4 Maximum velocity vectors of standing edge wave of $n=2$ mode

The velocity field of the standing edge waves will be more precisely explained. Figure 4 shows the maximum velocity vectors of the standing edge wave of $n=2$ mode at various points. The onshore-offshore velocity component should be equal to zero at every antinode in the offshore direction and on the nodal lines normal to the shoreline, according to Eq. (26). The longshore velocity component should be equal to zero at every antinode in the longshore direction and along the nodal lines parallel to the shoreline, according to Eq. (27). Therefore, u and v components must be simultaneously equal to zero at every point of interserection of nodal lines and at every antinode in the sence of the three dimensions. At the other points, where both u and v are not equal to zero, the phase relationship between these velocity components is always in phase and the ratio of these velocity components is held constant

for any time. That is, by using Eqs. (26), (27) and (22), the ratio of u to v is obtained as

$$\frac{u}{v}=\mathrm{B}\tan k_n y, \tag{37}$$

where

$$\mathrm{B}=-\frac{S}{\sqrt{n(n+1)}}\frac{1}{\mathrm{F}}\frac{\mathrm{dF}}{\mathrm{dS}}. \tag{38}$$

Then the ratio of u to v depends on a location, not on a time. Further, at the points where the value of Eq. (37) is positive, the phase difference between u and v is equal to zero, while at the other points it is equal to 180 degrees. **Figure 5** shows the spatial distribution of the phase difference for the edge wave of $n=2$ mode, which looks like a distorted checker.

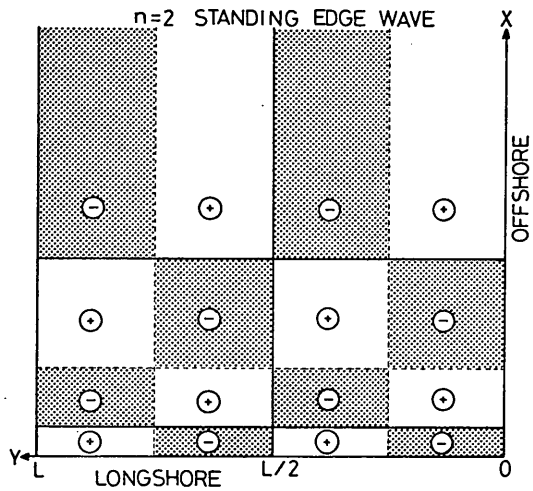

Fig. 5 Spatial distribution of phase relationship for standing edge wave of $n=2$ mode. A figure ⊕ means that phase difference is zero and ⊖ means that it is 180 degrees

The ratio of u to v at the shoreline ($S=1$) is derived by using Eqs. (30) ~(36) as

$$\left.\frac{u}{v}\right|_{S=1}=-\sqrt{n(n+1)}\tan k_n y. \tag{39}$$

Equation (39) means that the ratio of u to v becomes smaller for the edge waves of lower mode. Saying it differently, the longshore velocity component (v) which induces the longshore transport of sediments becomes relatively greater for the edge waves of lower mode. Then the edge waves of lower mode seem to be more probable to build up the beach cusps.

2.2 Examples of edge waves measured in the field

The field observations of the edge waves were begun in the 1970s. In this section, the edge waves observed by other researchers are explained with

examples.

Probably Huntley & Bowen[12] were the first to detect the edge waves in the field. The observation was carried out in August, 1972 at the center of Slapton Beach, South Devon, which was formed of a shingle ridge running in a concave curve for more than 5 kilometers. The beach profile in the intertidal zone was approximated by

$$h=7.05[1-\exp(-0.0314x)].$$

The offshore (u) and the longshore (v) components of the current velocity were measured by an electromagnetic currentmeter (E.M.C.) which was held at 0.3 meter above the sea bed. By utilizing the shift of the shoreline due to the change of the tide level, the measurements were repeated four times under the different distances from the shoreline to the currentmeter. As the results of cross-spectral analyses of four pairs of current data, a rather sharp peak at about 0.1 Hz, about one half of the incident wave frequency, was acknowledged in each of the spectra. The energy density at 0.1 Hz decreased exponentially with the offshore distance, being in agreement with curve predicted by Ball's theory. Moreover, the phase relationship between u and v components was found to be in phase. Then, they concluded that this energy peak was caused by the standing edge wave. This edge wave was not the cut-off mode but $n=0$ mode. Besides, the oblique angle of approach of the incident waves was about 10 degrees from the normal to the breaker line. And there were no obvious variation in the longshore topography.

Huntley[13] measured the u and v components of the current velocities by using three electromagnetic currentmeters, placed along a line normal to the shoreline, at Hell's Mouth Bay, England, in May, 1973. Measurements were made at about 1 kilometer from the southern end of the beach of 5.57 kilometers longshore length. Although there existed two longshore bars, the beach profile could be approximated by

$$h=3.5[1-\exp(-0.01x)].$$

Spectral analyses of each current component showed that the same energy peaks existed at the four frequencies which were lower than that of incident waves. Those four frequency of energy peaks satisfied the Ball's cut-off mode (Eq. 29) for $n=1\sim4$. And the decay of the velocity component of each mode with the offshore distance agreed with those predicted by Ball's theory. Since the phase relationships between u and v components of each currentmeter were in quadrature according to the cross-spectral analyses, these energy peaks were considered to be due to the progressive edge waves. The amplitudes of the longshore currents at the four peak frequencies were calculated from the energy spectra and were nearly same for each other. Then it was concluded that the amplitude of the edge wave of each mode was constant and showed no consistent trend with the modal number.

Sasaki & Horikawa[14] measured the waves in the surf zone in August 29, 1976 at Ajigaura Beach, Japan. The average beach slope up to 2 meters depth is about 1/60. Eleven wave staffs were arrayed in an area that covered 200 meters alongshore and 140 meters offshore around a open pile pier. The water surface fluctuations at these staffs were filmed with syncronized 16 mm motion-picture cameras, Bolex H16-SBM, with the speed of one frame per one second. As the results of cross-spectral analyses of these wave data, the several peaks of energy spectra were found. At these peak frequencies, the phase relationships and the coherences between each pair of two wave data were in phase and high. They concluded that these energy peaks were caused by the standing edge waves. And the locations of the nodal lines normal to the shoreline were detected. Equation (29) for the cut-off frequency was applicable to these peak frequencies for the edge waves of $n=1\sim6$ mode, by considering that αk_0 tends to $\tan\beta$ when k_0 tends to infinity.

Holeman, Huntley & Bowen[15] measured the current velocities in the surf zone by using three electromagnetic currentmeters at Martinique Beach, Canada, in August, 1976. This beach had a fairly simple topography with an almost linear profile of beach slope of 1/50. The slightly concaved shoreline of 2 kilometers length is terminated at one end by a headland and at the other by a reef extending 250 meters offshore. A second reef divides the length of the beach in the ratio 2 : 1. The three electromagnetic currentmeters were mounted 0.5 meter above the sea bed in the surf zone. Incident wave conditions varied from calm to swell and wind waves generated by a hurricane during one week observations. Throughout the storm the spectra of all three measurements of u components were dominated by a strong 0.01 Hz peak which remained constant in frequency despite significant changes in the incident wave field. Cross-spectral analyses between the u components of the different currentmeters clearly showed that the coherence was high and phase lag was 0 ± 11 degrees at 0.01 Hz. The spectra of v components, however, did not show the peak at 0.01 Hz clearly, because the positions of the currentmeters were located near the points of zero longshore current predicted by the theory of the edge waves. They concluded that this 0.01 Hz energy peak was caused by the standing edge wave of $n=1$ mode, and the frequency selection mechanism did not depend on the offshore beach topography, or the cut-off mode, but on the longshore topography with the headland and the reefs. Another observation at this place, when the beach slope was changed to 1/20, also revealed the existence of the standing edge wave of $n=1$ mode with the same longshore wavelength as this one.

Huntley & Bowen[4] simultaneously measured the u, v and vertical components of the current velocities by using three electromagnetic currentmeters at a single location at Queensland Beach, Canada, in September, 1976. The

Table 2 Examples of edge waves measured in the field

	Study site	Date	Instruments	Mode of edge waves
Huntley & Bowen[12]	Slapton Beach	1972.8.	one electromagnetic currentmeter	standing
Huntley[13]	Hell's Mouth Bay	1973.5.	three electromagnetic currentmeters	progressive
Sasaki & Horikawa[14]	Ajigaura Beach	1976.8.	16mm motionpicture cameras	standing
Holman, Huntley & Bowen[15]	Martinique Beach	1976.8.	three electromagnetic currentmeters	standing
Huntley & Bowen[4]	Queensland Beach	1976.9.	three electromagnetic currentmeters	standing

average beach slope around the measured point was about 1/13. As the results of cross-spectral analyses of these velocity components, the sharp peak at about one half of the incident wave frequency was found in each of the spectra. Since at this frequency the phase relationship between each pair of these velocity components was always in phase, this energy peak was considered to be due to the subharmonic standing edge wave. And the offshore decay of the amplitude of the velocity components, which were obtained by measuring at different shoreline positions, agreed well with the theoretical trend of the edge wave of zero mode. Towards the end of the measurement period, the beach cusps began to be formed at the shoreline, whose longshore spacing almost agreed with the one half of the longshore wavelength of the edge wave predicted for zero mode.

The above examples of the field observations are summerized in **Table 2**. In the past field observations for the edge waves, the wave profiles by 16 mm motion-picture cameras or the current components by electromagnetic current-meters were measured at several points in the surf zone. The method to extract the edge waves from the data obtained were to examine the energy peak frequency, the coherence, the phase relationship and the diminishing characteristics of the energy peak with the offshore distance through the cross-spectral analyses. But it was not explained clearly why the standing edge waves existed at the center of the beach without definite boundaries and why the progressive edge waves existed on the beach relatively near the boundaries, such as the headland, in the longshore direction.

A review of these papers may give an impression that the edge waves cannot be observed by the method other than those used in the past, mainly by electromagnetic currentmeters. In the previous observations, the attentions were mainly paid to the features of the edge waves along a line normal to the shoreline. The phase relationships between u and v of the edge waves are

clear and the wave heights and the current velocities decrease with the offshore distance. But the features of the edge waves which are more important than onshore-offshore characteristics are that the amplitude of the edge wave is maximum at the shoreline, as can be seen from the hypergeometric function having the maximum value at the shoreline, and that the water surface elevation of the edge wave varies sinusoidally in the longshore direction. For the edge waves have engineeringly become of major interest lately in connection with the littoral topography and the nearshore currents. These important features of the edge waves have been measured in the laboratory[16], but not in the field to the author's knowledge.

3. Field observation

3.1 Site of field observation (Sendai Beach)

The field observation was carried out at Sendai Beach during the periods of September 18 to 20, 1979. This beach is located in the north end of a bow-shape sandy coast of about 50 kilometers long facing to the Pacific Ocean, and is adjacent to the south breakwater of Sendai Port (see **Figs. 6** and **7** and **Photo. 1** in a frontispiece). The works of construction of the south breakwater were begun in the spring of 1968 with dumping of the rubble stones. The rubble mound breakwater of 400 meters long from the shoreline had been constructed by the spring of 1970. After the south breakwater had been prolonged more than 400 meters and its structure was changed to the composite

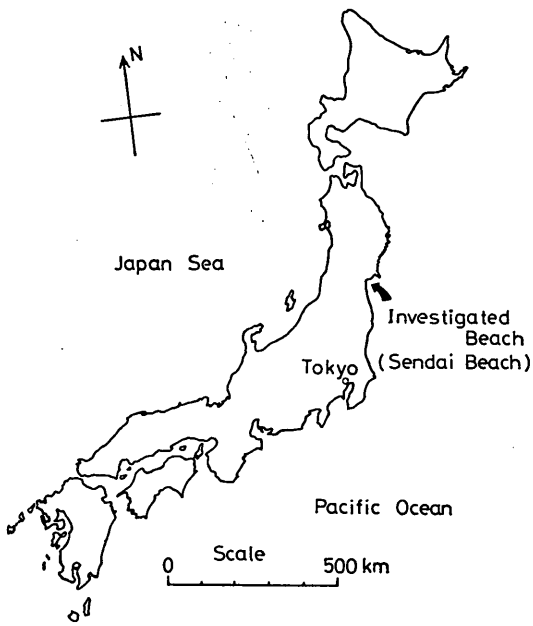

Fig. 6 Location of investigated beach

type, the beach at the base of the breakwater was seriously eroded localy due to the concentration of energy of waves reflected by the breakwater[17]. In order to prevent the erosion, a wing breakwater of 80 meters long from the bending corner of the breakwater was constructed with the concrete blocks during the period of February, 1977 to February, 1979. This wing breakwater is normal to the breakwater and is parallel to the shoreline. During the construction of the wing breakwater, the concrete blocks and rubble stones which were waste materials of the restoration works after the Sendai Earthquake on June 12, 1978 were put on the beach at the base of the breakwater for the purpose of both disposal of these scraps and prevention of further beach erosion.

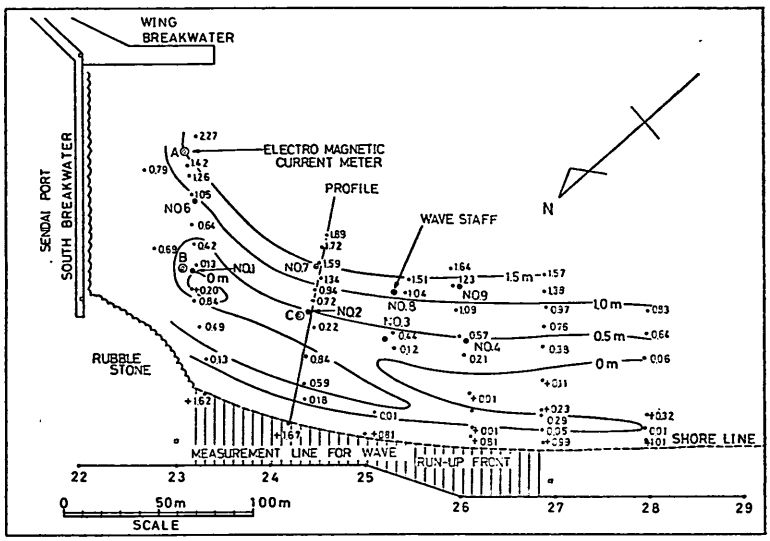

Fig. 7 Sea bottom topography of investigated site relative to datum line and measurement points of waves and current velocities

Figure 7 shows the sea bottom topography of the investigated site relative to the datum line as well as the shoreline during the measurements of the edge waves. The topography was surveyed using a surveyor's staff held by frog-men in the surf zone, the level of which was read from the land and the location of which was decided based on the angle data measured from two points on the land. The real water depth in the surf zone, ignoring the effects of a wave set-up and set-down, is the sum of figures in Fig. 7 and the tide level above the datum. There is a longshore bar about 50 meters offshore elongated from the south to the breakwater. Although the contours are not shown for lack of surveyed data, this bar, in turn, extends offshore along the breakwater as can be seen in Photo. 1 (in a frontispiece) with a light brown tone. The water depth above the longshore bar becomes deeper gradually

from the south towards the breakwater, and then shoals in front of the rubble stone area. A trough is formed on the land side of the longshore bar. Paying attention to the contours of 0 and 0.5 meter, this trough becomes deeper and wider gradually from the area in front of the reference point No. 28 towards the breakwater. Generally speaking, the contours are almost parallel to the shoreline.

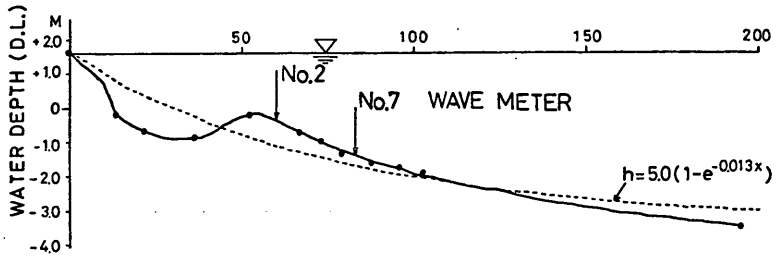

Fig. 8 Sea bottom profile at the center of investigated site

Figure 8 shows the sea bottom profile at the center of the investigated site along a solid line in **Fig.** 7. The sea bottom profile with the longshore bar about 50 meters offshore from the shoreline can be approximated by

$$h=5.0[1-\exp(-0.013x)], \tag{40}$$

as shown by a dashed line in **Fig.** 8.

3.2 Measurements of waves and currents in the surf zone.

The observation for the edge waves was carried out for about one hour around 15 o'clock on September, 18. It was just at a high tide with almost no change of the tide level of 1.52 meters above the datum line. Another observation was carried out at a low tide with the tide level of 0.64 meter on September, 19, but resulted in failures, because the wind velocity from the offshore became too large after lifting a balloon and only several aerophotographs could be taken.

The offshore waves and wave direction were measured with the existing ultra-sonic wave meter and ultra-sonic currentmeter at the depth of 20 meters under the datum line.

In order to measure the water surface fluctuations in the surf zone, eight wave staffs were arrayed in approximately two parallel alignment to the shoreline as shown in **Fig.** 7. The water surface fluctuations at these staff were filmed with four 16 mm motion-picture cameras, Bolex H16-SMB, at one second interval for the duration of about one hour. The set of shutter of the four cameras were controled synchronously. After the films had been developed, they were projected one by one frame on a screen, from which the levels of the water surfaces were read with a scale. The measured data of the wave profiles may have contained some errors owing to the following reasons:

(1) Since the distance from the cameras set above the shoreline to the wave staffs were in the order of 60~80 meters, the graduations on the staffs

can hardly be seen on the screen. Then, the levels of the water surfaces are read with the scale by interpolating the distinct length of the wave staffs.

(2) The wave staffs were occasionally hidden by the wave crests.

(3) There were sprays of water due to the wave breaking.

(4) The wave staffs seemed to incline a little at the author's glance from the land. But angles of inclination of the wave staffs were not measured.

The Lagrangian velocity of currents in the surf zone were measured by tracking twenty floats, which were released in the surf zone by frog-men. The float has a shape of a rectangular parallelpiped of 1 meter long, 1 meter wide and 0.8 meter high, and is made of canvas. The float is filled with the sea water inside it. In order to provide the float with a small amount of buoyancy, a soft urethane sheet of 1 meter long, 1 meter wide and 0.01 meter thick is attached to the upper surface of the float. The float is colored in red, yellow or green. This type of the float can move precisely with the currents without riding on the waves in the surf zone. The positions of the floats were taken in a series of aerophotographs by a Hasselblad 500EL motor-driven camera (60mm) mounted on a balloon lifting at an altitude of around 500 meters from the time 14 hours 24 minutes to 15 hours 22 minutes on September 18 (see **Photo. 2-a,b,c** in a frontispiece). The camera was triggered by a radio transmitter from the ground at the intervals of about thirty seconds for initial 19 frames and about sixty seconds for remaining 50 frames. These frames were projected on a screen with adjustment of an optical axis of the camera being normal to the screen by utilizing signals on the ground. The Lagrangian velocity vectors of the surface currents were obtained by deviding the horizontal distance of the same float on the series of aerophotographs by the respective photographing interval.

The two horizontal components of the Eulerian velocity were measured by three electromagnetic currentmeters of two-component type at the three points indicated by A, B and C in Fig. 7. The three electromagnetic currentmeters were held at the elevations of 0.20 meter (A), 0.25 meter (B) and 0.23 meter (C) above the sea bed, respectively. The horizontal directions of the fixation of these currentmeters were measured with a magnet compass in the sea water. The data of these velocities were recorded on an analogue magnetic tape and digitized at the interval of 0.1 second. Every ten consecutive digital data were averaged to yield the smoothed data with the time interval of 1 second.

Further details of the investigated site and the method of observation can be found elsewhere[18].

3.3 General features of waves and currents at the investigated site

The spectra of the offshore waves and of the waves at the points of No. 1 and No. 2 are shown in Fig. 9. A sampling interval of data is Δt=1 second

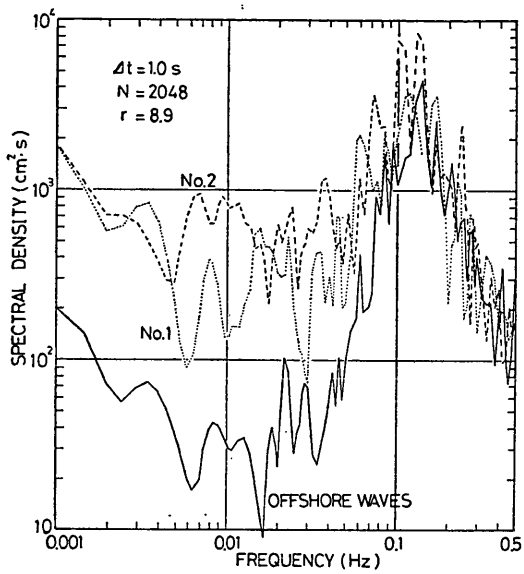

Fig. 9 Spectral densities of offshore waves and of waves at points No. 1 and No. 2

and a number of data is N=2048. The equivalent degree of freedom with a filter used for smoothing is r=8.9. For each of the spectrum the most prominent peak occurs at about 0.13 Hz (periods 7.7 seconds). The peak energy density of the waves at No. 2 is slightly greater than those of the offshore waves and the waves at No. 1. This is because the point of No. 2 was located at the seaward site of the surf zone as seen in **Fig. 11**, where the incident

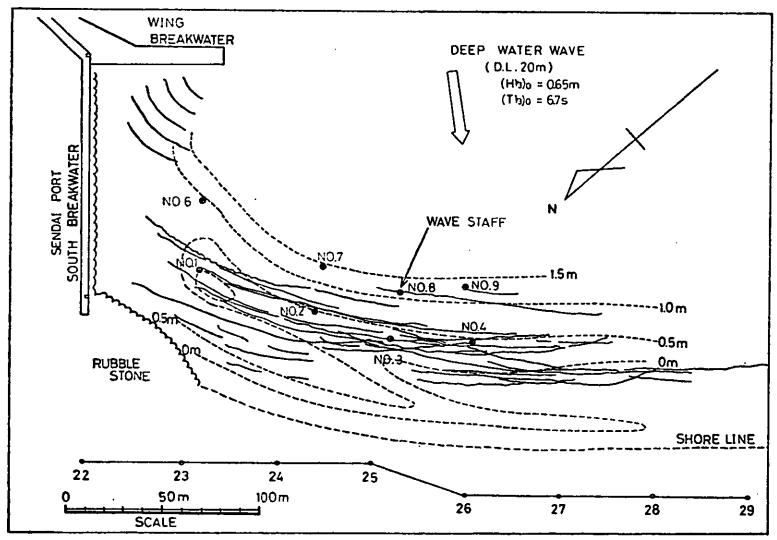

Fig. 10 Wave crest lines and direction of offshore waves during observation

waves become maximum in height. Another outstanding feature of these spectra is that the energy densities of the waves at the points of both No. 1 and No. 2 are about ten times as much as that of the offshore waves at the frequency lower than 0.05 Hz. From this feature, it is evident that the wave energy of the low frequency is trapped in the investigated area.

The offshore wave direction which is shown with an open arrow in Fig. 10 was calculated with the following equation for the principal wave direction[19] by using two components of the horizontal velocity measured by the ultra-sonic currentmeter at the depth of 20 meters under the datum line.

$$\tan 2\theta = \frac{2\overline{uv}}{\overline{u^2} - \overline{v^2}}. \tag{41}$$

Wave crest lines in the surf zone were read from the aerophotographs on which the crest lines are clearly noticed, and are shown superimposingly in Fig. 10. As seen in Fig. 10, the wave crest lines were almost parallel to the shoreline. That is, the incidence angle of waves was almost normal to the shoreline in the surf zone.

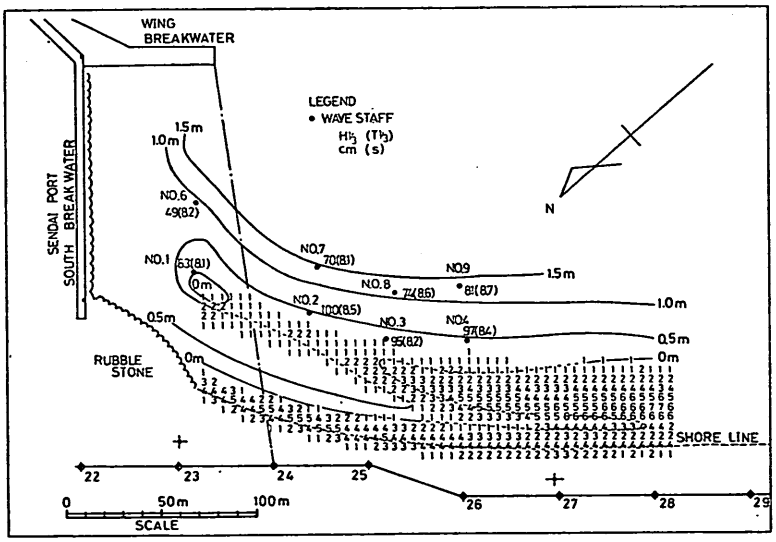

Fig. 11 Spatial distribution of rate of white foams (read from aerophotographs) and wave heights and periods

The white foams on the water surface are seen in the surf zone on all of the aerophotographs. Figure 11 shows the spatial distribution of the rate of the white foams in the surf zone. For example, the figure 4 in Fig. 11 means that the white foams can be seen in 40 percent of all aerophotographs at such point. As the white foams on the water surface are due to the wave breaking, this figure is considered to be the spatial distribution of the rate of the wave breaking. As can be seen in Fig. 11, the waves broke at the slightly landward

of the longshore bar. The rate of wave breaking decreased gradually in the longshore direction towards the south breakwater, and finally increased a little in front of the rubble stone area. This trend correspoded to the variation of the water depth on the longshore bar except near the point No. 2, where the rate of wave breaking was slightly large with the value of 20 percents.

Table 3 Mean wave heights and periods and mean water depths in the surf zone and at the offshore

	number of waves	max.		1/10		1/3		mean		water depth (m)
		height (m)	period (s)	height (m)	period (s)	height (m)	period (s)	height (m)	period (s)	
No. 1	475	1.19	10.4	0.82	8.3	0.63	8.1	0.39	6.3	1.41
No. 2	446	1.90	10.1	1.29	8.6	1.00	8.5	0.60	6.7	1.79
No. 3	431	1.74	6.2	1.25	8.2	0.95	8.2	0.58	7.0	1.69
No. 4	452	1.70	9.0	1.25	8.5	0.97	8.4	0.59	6.6	1.88
No. 6	494	1.10	5.6	0.63	8.9	0.49	8.2	0.31	6.1	2.21
No. 7	463	1.39	9.5	0.89	8.1	0.70	8.1	0.45	6.5	2.48
No. 8	445	1.48	8.3	0.95	8.7	0.74	8.6	0.47	6.7	2.49
No. 9	420	1.34	8.2	1.02	8.8	0.81	8.7	0.52	7.1	2.40
offshore waves	478	1.12	9.7	0.83	7.2	0.65	6.7	0.42	5.2	21.52

Both the significant wave heights and periods were calculated by the zero up-crossing method by using 3600 data of the time interval of one second for each point, and are shown in **Fig. 11**. Other mean wave heights and periods as well as the mean water depth at the wave staffs are listed in **Table 3**. The significant wave periods of all points were in the order of 8.1~8.7 seconds, which was longer than that of the offshore waves, 6.7 seconds. The significant wave heights at the points of No. 2, 3 and 4 were about 1.0 meter and can be considered to be the same heights with one another, because the data of waves are subjected to the statistical variation and contain some errors, as was stated previously. On the other hand, the significant wave heights at the point No. 1 was apparently lower than those at the points No. 2, 3 and 4. And the significant wave heights at the point No. 6 was also lower than those at the points No. 7, 8 and 9. This means that the points both No. 1 and 6 were located in the area sheltered by the wing breakwater and the other points were located in the area where the waves directly came from the open sea. A boundary between these area is shown in **Fig. 11** by a dash-dot line connecting the tip of the wing breakwater and the reference point No. 24.

Figure 12 shows the velocity vectors of the surface currents measured by tracking the floats. The magnitude of velocity is indicated with the length of vector as shown in the legend. The floats were released at the point of southern side of No. 4 at first and at the point offshore of No. 8 later. All of the floats moved to the vicinity of the shoreline, gradually changing their directions

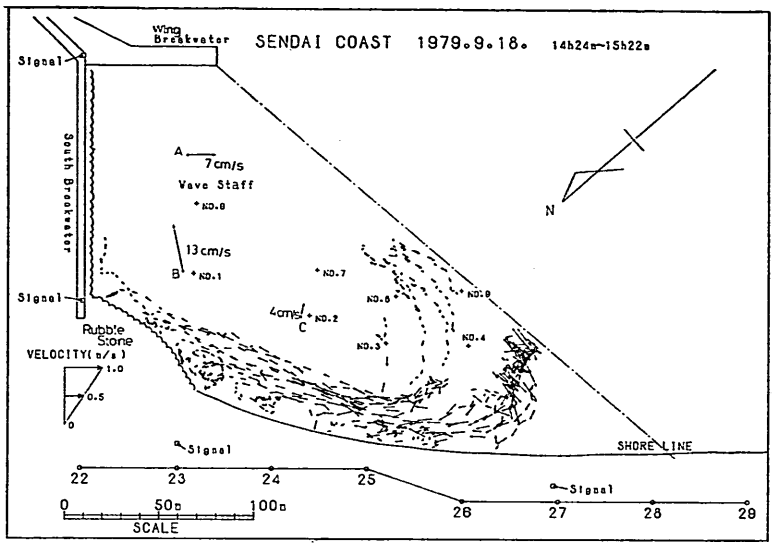

Fig. 12 Nearshore current pattern behind wing breakwater

in clockwise, where they changed their direction such as towarding the south breakwater. After that, the floats moved parallel to the shoreline inside a zone between the shoreline and about 30 meters offshore. A longshore current velocity was high with the maximum speed of 0.5 meter per second and the average speed of 0.3 meter per second. According to the visual observation, this fast currents always existed during the five days of field study.

In Fig. 12, the mean current velocities of the lower layer which were measured by the three electromagnetic currentmeters are also shown at the points A, B and C. The magnitude of the current velocities at these points are indicated by figures beside each arrow, not following the legend. The results of measuring the currents with the floats and by the electromagnetic currentmeters indicate the existence of large clockwise circulation behind the wing breakwater. This circulation was spreaded in the whole area which is bounded by a dashdot line connecting the tip of the wing breakwater and the shore in front of the reference point No. 28, as shown in Fig. 12.

No rip current was detected by tracking the floats in the investigated area. But the author confirmed the existence of a rip current by the visual observation at the slightly right side of the reference point No. 29.

4. Examination of edge waves in the field

4.1 Wave run-up fronts

The amplitude of incoming waves is minimum at the shoreline because of wave attenuation due to the wave breaking, the turbulence and the bottom friction in the surf zone. On the other hand, the amplitude of the edge wave

is maximum there as can be seen from the hypergeometric function having the maximum value at the shoreline. Thus, the effects of the edge waves are expected to emerge noticeably in the run-up phenomena on the foreshore.

The typical examples of the aerophotographs are shown in **Photo. 2** (in a frontispiece). In these aerophotographs and the remaining ones, the positions of wave run-up fronts are clearly noticed as the landward edges of narrow white zones on the foreshore. And it is also noticed in the photographs that the positions of wave run-up fronts vary in the longshore direction. If these longshore variations were due to the edge waves, the edge waves are detected in these phenomena.

Since the investigated site is adjacent to the south breakwater of Sendai Port, the edge waves should be the standing ones. Then, from Eqs. (22) and (25) for the standing edge wave, the profile of edge wave in the longshore direction at the shoreline is described as

$$\zeta(0,y,t)=A(0)\sin k_n y\cdot\sin\sigma_n t, \tag{42}$$

$$A(0)=a_n, \tag{43}$$

where the subscript n denotes the modal number of the edge wave and a_n is the shoreline amplitude of the standing edge wave. Therefore, the horizontal position of run-up front from the shoreline due to the standing edge wave is described as

$$R_n(y,t)=\frac{a_n}{\tan\beta}\sin k_n y\cdot\sin\sigma_n t, \tag{44}$$

where $R_n(y,t)$ is the horizontal position of wave run-up front from the shoreline and $\tan\beta$ is the slope of the foreshore. If the edge waves of various modes and different periods coexist at the same time in the investigated site, the position of wave run-up front which is a result of superposition of these edge waves will vary randamly in the longshore direction at any given time. In this case, an expression which may be able to describe the longshore variation of wave run-up front is

$$R(y,t)=\sum_n\frac{a_n}{\tan\beta}\sin(k_n y+\varepsilon_n')\sin(\sigma_n t+\varepsilon_n''), \tag{45}$$

where $R(y,t)$ is the horizontal position of run-up front from the shoreline due to the standing edge waves of various mode and ε_n' and ε_n'' are phase lags of a longshore location and a time, respectively.

Only the left hand side of Eq. (45), $R(y,t)$, is measurable in the series of the aerophotographs. For the purpose of measuring the wave run-up fronts on the foreshore from the aerophotographs, 37 measurement lines shown in **Fig. 7** are set up with the longshore interval of 5 meters except for the rubble stone area at the base of south breakwater. The measurement lines are normal to a base line that connects two reference points No. 22 and 25 or No. 26 and 29. As Huntley[13] pointed out, it is difficult to find the shoreline which is the time

mean position of wave run-up fronts. Therefore, the horizontal positions of wave run-up fronts from the base line are read along the each measurement line from the aerophotographs in the same manner as the case of float tracking. A accuracy of measurement for reading positions is 0.5 meter. A number of the aerophotographs to be utilize for this purpose is 66 out of 69, because the foreshore is not taken enough in the three aerophotographs of remaining. After that, a time-averaged position of run-up front was calculated on each measurement line. And the positions of wave run-up fronts from the shoreline were obtained by taking account of these time-averaged positions.

A dashed line in Fig. 7, which connects the time-averaged positions of wave run-up fronts on the measurement lines, can be considered as the shoreline during the observation. Since this shoreline is smooth in the longshore direction, there exsisted neither a irregular nor a rhythmic topography on the foreshore. As a matter of fact, the beach was smooth in the longshore direction as far as the author's visual observation could be made. Therefore, the longshore variation of wave run-up front dose not involve the effects of the topography.

Since it was just at a high tide with almost no change of the tide level when the observation was carried out, the characteristics of the edge waves are concidered to be constant during the measurements[20].

4.2 Empirical eigenfunctions

Equation (45) is similar to the Fourier series expansion in the sense that $R(y,t)$, which is the only measurable value, is expressed by superimpose of trigonometrical functions. But it is unknown whether the measured value $R(y,t)$ is immediately expanded in a series of the trigonometrical functions or not. For it is impossible to know in advance whether the standing edge waves do exist or not, and it may well be that other phenomena than the edge waves contribute to the longshore variation of wave run-up front. If we assume the other possible phenomena being independent and irrelevant each other, we can use a generalized expression for $R(y,t)$ as in the following by introducing unknown orthgonal functions $E_n(y)$ in stead of the trigonometrical functions:

$$R(y,t)=\sum_n C_{n,t}\cdot E_n(y), \tag{46}$$

where

$$C_{n,t}=\frac{a_n}{\tan\beta}\sin(\sigma_n t+\varepsilon_n''). \tag{47}$$

Now, let the measument lines be numbered for 1 to n_y in the longshore direction and let the measurement time be numbered for 1 to n_t in sequence of measurement, where the longshore intervals and the time intervals of measurements are not necessarily constant, respectively. And let $R(y,t)$ denote the horizontal position of wave run-up front on the y-th measurement line at the t-th measurement time. Since $R(y,t)$ is the horizontal position of wave

run-up front from the time-averaged position, a equation of

$$\bar{R}(y)=\frac{1}{n_t}\sum_{t=1}^{n_t}R(y,t)=0, \tag{48}$$

is valid.

The longshore variation of wave run-up front at the t-th measurement time is expressed by the discontinuous values, which forms a vector

$$\boldsymbol{R}_t=(R(1,t),R(2,t),\cdots\cdots,R(n_y,t))^T, \tag{49}$$

where T is a transpose operator. If we express the unknown orthogonal functions $E_n(y)$ by unknown orthogonal vectors $\boldsymbol{e}_n$ of the discontinuous values, Eq. (46) becomes

$$\boldsymbol{R}_t=\sum_n C_{n,t}\cdot\boldsymbol{e}_n+\boldsymbol{\varepsilon}_t,(t=1\sim n_t), \tag{50}$$

where the vector $\boldsymbol{\varepsilon}_t$ contains not only the error in the measured values $\boldsymbol{R}_t$ but also the factors of small effects at the t-th measurement time. The method of estimating the model structure of Eq. (50) from the measured values $\boldsymbol{R}_t$ is called a factor analysis. The criterion of estimation of this model structure, however, cannot be defined uniquely, because there are unknown values altogether in the right hand side of Eq. (50). Because of this, assuming $\boldsymbol{\varepsilon}_t=0$ and the number n varies from 1 to n_y, Eq. (50) reduces to

$$\boldsymbol{R}_t=\sum_{n=1}^{n_y}C_{n,t}\cdot\boldsymbol{e}_n. \tag{51}$$

This new model structure can be easily estimated by a principal component analysis as follows.

At first, by using the measured values ($\boldsymbol{R}_t$) we have to calculate a symmetric correlation matrix A which is formed with the elements

$$a_{ij}=\frac{1}{n_y\cdot n_t}\sum_{t=1}^{n_t}R(i,t)\cdot R(j,t). \tag{52}$$

The matrix A possesses a set of eigenvalues λ_n and a set of corresponding eigenvectors $\boldsymbol{e}_n$ which are defined by a matrix equation

$$\mathbf{A}\boldsymbol{e}_n=\lambda_n\boldsymbol{e}_n, \qquad (n=1\sim n_y). \tag{53}$$

This equation has to be solved numerically by employing an electronic computer to yield λ_n and $\boldsymbol{e}_n$ with the matrix algebra. Since the matrix A is a real symmetric one,

$$\left.\begin{aligned}&\lambda_n\geqq 0\\ \text{and}\quad&\\ &\boldsymbol{e}_p^T\boldsymbol{e}_q=\delta_{pq}\end{aligned}\right\} \tag{54}$$

should hold, where δ_{pq} is the usual Kronecker delta. The $\boldsymbol{e}_n$ in Eq. (53) corresponds to the $\boldsymbol{e}_n$ in Eq. (51). As the orthogonal function $\boldsymbol{e}_n$ can be empirically estimated by Eqs. (52) and (53) by using the measured value ($\boldsymbol{R}_t$), this $\boldsymbol{e}_n$ is called the empirical eigenfunction[10),11)].

By premultiplying Eq. (51) by $\boldsymbol{e}_n^T$, we have

$$\boldsymbol{e}_n^T\boldsymbol{R}_t=\sum_{m=1}^{n_y}C_{m,t}\boldsymbol{e}_n^T\boldsymbol{e}_m$$

$$=\sum_{m=1}^{n_y} C_{m,t}\delta_{n,m}$$

$$=C_{n,t}. \tag{55}$$

The scalar coefficient $C_{n,t}$ can be evaluated by this process. Ultimately, the model structure of Eq. (51) can be estimated only from the measured value $\boldsymbol{R}_t$.

In the principle component analysis, a contribution rate is defined by

$$\lambda_n \Big/ \sum_{n=1}^{n_y} \lambda_n, \tag{56}$$

as the criterion of the magnitude of λ_n.

4.3 Analysis of wave run-up fronts by means of empirical eigenfunctions

The empirical eigenfunctions have been computed by the method discribed above for the longshore variations of wave run-up fronts at Sendai Beach. As a number of the measurement lines is 37 ($=n_y$) and that of the measurement times is 66 ($=n_t$), a total number of data is 2442 ($=n_y \times n_t$). As should be expected, 37 sets of eigenvalues (λ_n) and eigenvectors (e_n) are obtained as a result of analysis. **Table 4** shows the resultant values of eugenvalues (λ_n), contribution rates and accumulation rates of contribution for $n=1$ to 20, and the sum of these values for $n=21$ to 37. This analysis, however, contains the errors and the small effects because of putting $\varepsilon_t=0$ in Eq. (50). Therefore,

Table 4 Eigenvalues, contribution rates and accumulation rates of contribution

n	eigenvalue	contribution rate (%)	accumulation rate of contribution (%)
1	4.266	50.70	50.70
2	2.181	25.92	76.61
3	0.722	8.58	85.19
4	0.358	4.25	89.45
5	0.218	2.59	92.04
6	0.177	2.10	94.14
7	0.093	1.11	95.25
8	0.072	0.86	96.10
9	0.066	0.78	96.89
10	0.053	0.63	97.52
11	0.044	0.52	98.04
12	0.034	0.40	98.44
13	0.025	0.30	98.74
14	0.023	0.27	99.01
15	0.014	0.17	99.18
16	0.009	0.11	99.29
17	0.009	0.11	99.39
18	0.007	0.08	99.48
19	0.006	0.07	99.55
20	0.005	0.06	99.61
21～37	0.033	0.39	100.00

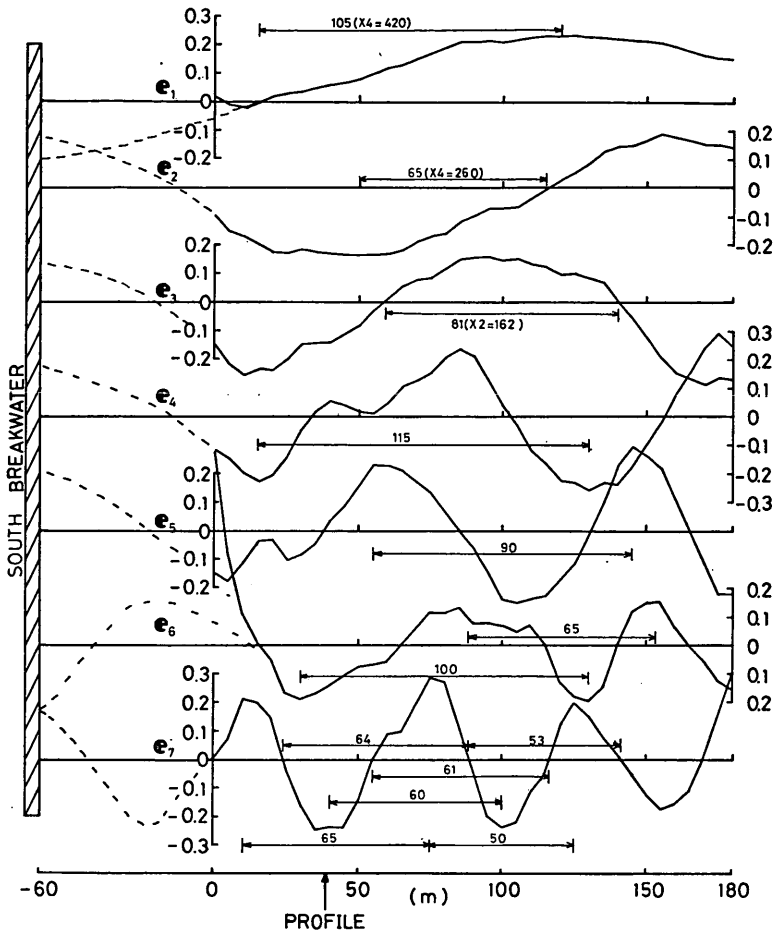

Fig. 13 Empirical eigenfunctions of $e_1 \sim e_7$

those the contribution rates smaller than 1%, as a temporary standard, have to be discarded from the results.

The eigenvalues and eigenvectors of remaining are $\lambda_1 \sim \lambda_7$ and $e_1 \sim e_7$, and the accumulation rate of contribution is 95.25%. These eigenfunctions ($e_1 \sim e_7$) are shown in Fig. 13. The features of this figure are as follows:

(1) Each eigenfunction except e_1 and e_2 varies sinusoidally in the longshore direction. Even e_1 and e_2, the wavelengths of which are long, can be considered to be parts of the sinusoidal variations.

(2) If each eigenfunction is extrapolated to the south breakwater through the rubble stone area as denoted by a dashed line in Fig. 13, the phase of each eigenfunction becomes nearly that of antinode at the south breakwater.

From these features of the eigenfunctions, it is concluded that the longshore variation of wave run-up front at Sendai Beach is formed by overlapping of many standing waves of different wavelengths with their antinodes positioned

Table 5 Eigenvalues, contribution rates, longshore wavelengths and periods for standing edge waves of $n=1$ to 7 modes

n	λ_n	contribution rate (%)	wavelength(m)	wave period (s)
1	4.266	50.7	420	60.0
2	2.181	25.9	260	37.1
3	0.722	8.6	162	23.1
4	0.358	4.3	115	16.4
5	0.218	2.6	90	12.9
6	0.177	2.1	82.5	11.8
7	0.093	1.1	58.5	8.4

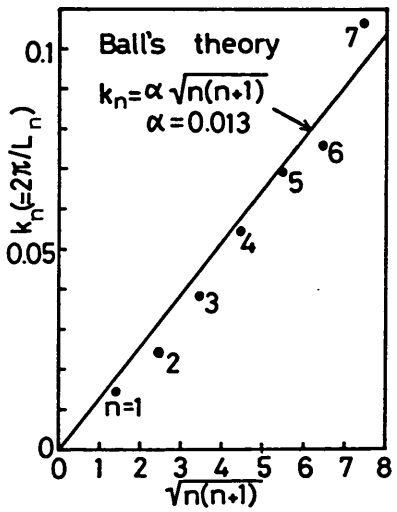

Fig. 14 Relation between longshore wave numbers and modal numbers for edge waves of cut-off mode

at the south breakwater. But it is open to question whether these standing waves are the edge waves or not.

The longshore wavelengths of these standing waves may be estimated as shown in Fig. 13. For e_1, e_2 and e_3, the wavelengths of which are long, either a quarter or a half of wavelength is read, while for e_6 and e_7 the mean wavelengths are calculated, respectively. The resultant wavelengths are listed in the third colum in Table 5. On the other hand, a wave number of the edge wave of n-th mode can be predicted by Eq. (28). By assuming the eigenfunction e_n corresponds to the standing edge wave of n-th mode, the wave number $k_n(=2\pi/L_n)$ obtained from Fig. 13 are plotted against $\sqrt{n(n+1)}$ as in Fig. 14 to examine the relation of Eq. (28). A solid line in this figure indicates Eq. (28) with $\alpha=0.013$

which is the exponential coefficient of the beach profile at the investigated site (see Eq. 40). Because the plotted data agree well with the solid line based on Ball's theory, it is concluded that the eigenfunction e_n corresponds to the cut-off mode of the standing edge wave of n-th mode.

Mention is made here for the value of k_6 which is smaller than the trend of whole data. As seen in **Fig. 13**, e_6 has a large positive value at the left hand end. The eigenfunction e_6 may have been affected by e_1 which has a positive value at the left hand end.

By using $C_{n,t}$ calculated by Eq. (55), it is possible in principle to examine the time variation of the empirical eigenfunction[10),21)]. Since the physical meaning of $C_{n,t}$ in this analysis is represented by Eq. (47), $C_{n,t}$ is expected to vary sinusoidally with respect to time. In the present study, however, we cannot examine the time variations of the empirical eigenfunctions by means of $C_{n,t}$, because the time interval of measurement is long. From Eqs. (28) and (29) for the dispersion relation for the standing edge wave of cut-off mode, we have

$$T_n=L_n/\sqrt{gk_0}, \tag{57}$$

where T_n is the period and L_n is the longshore wavelength of the standing edge wave of n-th mode. The period of each standing edge wave which is calculated by using Eq. (57) with the wavelength read from **Fig. 13** is shorter than 60 seconds as shown in the fourth column in **Table 5**. On the other hand, the interval of photographing is about 60 seconds for two-third of the whole data. That is to say, the measuring interval is longer than the periods of each standing edge wave.

We may assume here that all of photographing were carried out randomly for the phase of the standing edge waves, although the period of the standing edge wave of $n=1$ mode almost agrees with the photographing interval. Here, let us rewrite the subscript t by p in the ascending order of magnitude of the absolute value of $C_{n,t}$ for each modal number. That is,

$$0\leqq|C_{n,1}|\leqq\cdots\leqq|C_{n,p}|\leqq|C_{n,p+1}|\leqq\cdots\leqq|C_{n,66}|. \tag{58}$$

After these operation has been done for the coefficients, the time series data of $C_{n,t}$ is shuffled. For the newly defined coefficients, a equation of

$$|C_{n,p}|=\frac{a_n}{\tan\beta}\sin\left\{\frac{\pi}{2}\cdot\frac{1}{n_t}\left(p-\frac{1}{2}\right)\right\},\quad (p=1,\cdots,n_t) \tag{59}$$

is valid for each modal number in place of Eq. (47). Then, we have

$$\sum_{p=1}^{n_t}|C_{n,p}|^2=\left(\frac{a_n}{\tan\beta}\right)^2\sum_{p=1}^{n_t}\sin^2\left\{\frac{\pi}{2}\cdot\frac{1}{n_t}\left(p-\frac{1}{2}\right)\right\}. \tag{60}$$

By premultiplying Eq. (53) by $\boldsymbol{e}_n^T$ and by using Eq. (55), we have

$$\lambda_n(\boldsymbol{e}_n^T\boldsymbol{e}_n)=\boldsymbol{e}_n^T\mathbf{A}\boldsymbol{e}_n=\frac{1}{n_y n_t}\sum_{t=1}^{n_t}(\boldsymbol{e}_n^T\boldsymbol{R}_t)(\boldsymbol{e}_n^T\boldsymbol{R}_t)=\frac{1}{n_y n_t}\sum_{t=1}^{n_t}C_{n,t}^2. \tag{61}$$

From Eqs. (60) and (61), we have

$$\lambda_n=\frac{1}{n_y n_t}\sum_{t=1}^{nt} C_{n,t}^2=\frac{1}{n_y n_t}\sum_{p=1}^{nt}|C_{n,p}|^2=\frac{33}{n_y n_t}\left(\frac{a_n}{\tan\beta}\right)^2. \tag{62}$$

Therefore, the relation between the amplitude of the edge wave and the eigenvalue is obtained as

$$a_n=\tan\beta\sqrt{\frac{n_y n_t}{33}\lambda_n}. \tag{63}$$

Table 6 Resultant amplitudes of standing edge waves of $n=1$ to 7 modes

modal number	resultant amplitude (m)
1	2.73
2	1.95
3	1.12
4	0.79
5	0.62
6	0.56
7	0.40

With values of $\tan\beta=1/6.5$, $n_y\times n_t=2442$ and every eigenvalue listed in the first colum in **Table 5**, the amplitude of the standing edge wave of each mode was estimated and is listed in **Table 6**. The author's visual observations do not support these resultant values of the amplitudes which are apparently too large. The effect of incoming waves riding on the edge waves can be considered as one of causes for these large values. Although the amplitude of incoming waves is minimum at the shoreline because of wave attenuation in the surf zone, the energy of incoming waves is still left and is consumed in forcing the water to run up on the foreshore in the end. The remaining energy of incoming waves at the crests of the edge wave is greater than that at the troughs, because the water depth at the former is deeper than that at the later. Therefore, it is considered that the run-up phenomena due to the edge waves are exaggerated by the remaining energy of incoming waves. Because of this, the numerical values of the coefficient of Eq. (63) is not employed in the subsequent discussion.

Next, let us examine the relation between the eigenvalues and the wave numbers of the standing edge waves, which are listed in **Table 4**. **Figure 15** shows a plot of square root of eigenvalues ($\sqrt{\lambda_n}$) versus the wave numbers. Since the data are plotted well on a solid line, the following relation is obtained

$$\sqrt{\lambda_n}=0.034k_n^{-1}. \tag{64}$$

From Eqs. (63) and (64) by dropping the term of the coefficient, we have

$$a_n\propto k_n^{-1}, \tag{65}$$

or by using Eq. (57),

$$a_n \propto \sigma_n^{-1}. \tag{66}$$

Therefore, it becomes clear that the amplitude of the standing edge wave at the investigated site is inversely proportional to its wave number (or frequency).

This result of Eq. (65) or (66) is different from the result of the field observation by Huntley[13] who concluded that the shoreline amplitude of the edge wave was constant and showed no consistent trend with the modal number. The edge waves observed by Huntley were, as previously mentioned, the progressive ones at the beach 1 kilometer apart from the headland, while the edge waves of the present study are the standing ones which exist near the rubble mound breakwater of Sendai Port. It is considered that the standing edge waves are formed as a result of reflection of the progressive edge waves by the breakwater. Then, the reflection of the edge waves at the breakwater is examined in order to explain the difference between the results of the present study and Huntley's one.

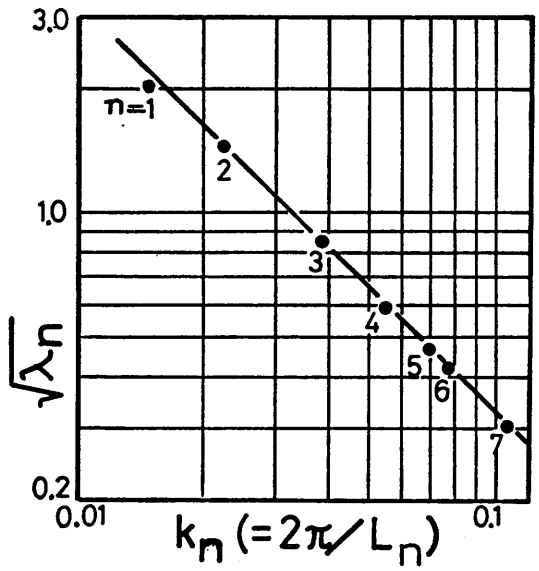

Fig. 15 Relation between eigenvalues and longshore wave numbers

Since the reflection coefficient of this breakwater is unknown, another experimental result by Tanimoto et al.[22] of a breakwater armored with wave dissipating concrete blocks which is somewhat structually similar to the breakwater in question is shown in **Fig. 16**. In this figure, the values of B_{bo}/L of the edge waves are also plotted on the horizontal axis. In this calculation, the wavelengths of the edge waves listed in the third colum in **Table 5** are used and the value of B_{bo} is assumed to be 6 meters which is read from the aerophotographs. The reflection coefficients of the edge waves of high mode

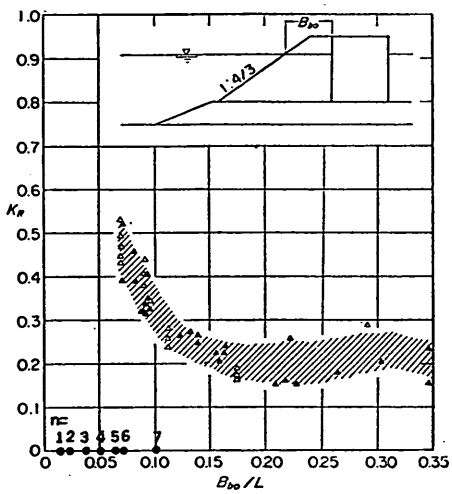

Fig. 16 Reflection coefficient of breakwater armored with wave dissipating concrete blocks (Tanimoto et al. [22])

are about 0.4~0.5. Although the data of the edge waves of low mode are plotted beneath the scope of the experimental result, it is expected from the feature of the experimental result that the reflection coefficients of the edge waves of low mode are nearly 1.0. Therefore, the energy of the edge waves of high mode is more dissipated by the breakwater than that of low mode. As the result, the amplitude of edge wave decreases with the decrease of the wavelength, or with the increase of the wave number.

Equation (59) suggests that $|C_{n,p}|$ is a trigonometrical function of p. In order to examine this feature of $|C_{n,p}|$, let $|C_{n,p}|$ be standardized by $|C_{1,p}|$ as

$$|C'_{n,p}| = \frac{\sum_{p=1}^{n_t} |C_{1,p}|}{\sum_{p=1}^{n_t} |C_{n,p}|} \cdot |C_{n,p}|. \tag{67}$$

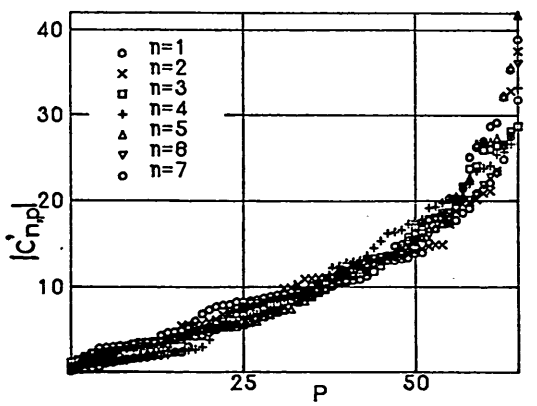

Fig. 17 $|C'_{n,p}|$ for each modal number

Figure 17 shows $|C'_{n,p}|$ for each modal number. As seen from **Fig. 17**, the evey increasing trend of $|C'_{n,p}|$ with p is independent on the modal number n, but depends on p. That is to say, it can be considered that the time variation of $C_{n,t}$ is statistically same for each other. **Fig. 17**, however, unexpectedly shows that $|C_{n,p}|$ is not apparently the trigonometrical function of p. The causes which lead to the problem are considered as follows:

(1) It is in horizontal position that the wave run-up front is measured.

(2) The beach slope of foreshore is not exactly constant.

(3) The run-up phenomena is considered to contain the effect of incoming

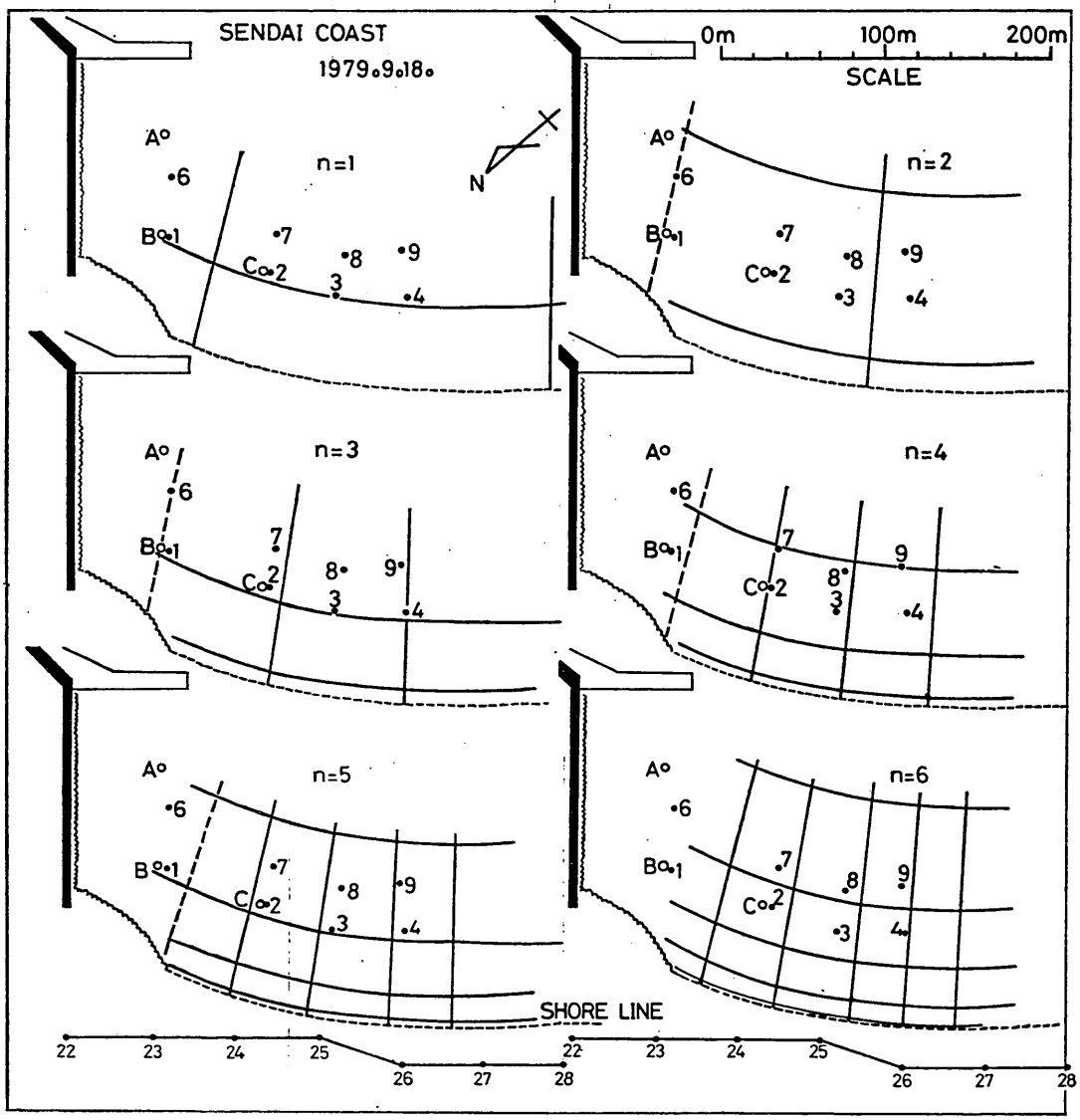

Fig. 18 Positions of nodal lines for standing edge waves of n=1 to 6 modes at Sendai Beach

waves as previously mentioned.

(4) The theoretical treatment of the boundary at the shoreline is not definite in the theory of the edge waves.

But these causes were not examined in detail and are remained to study in future to determine the amplitude of the edge waves.

Through the above analysis, it becomes clear that the standing edge waves which correspond to the cut-off mode predicted by Ball's theory exist at the investigated beach. Then, the nodal lines of the standing edge wave of each mode should exist in both the offshore and the longshore directions. The positions of nodal lines parallel to the shoreline are determined by the offshore distance from the shoreline (x) with which the hypergeometric function (Eq. 22) equals to be zero, and a number of these lines is as same as the modal number. On the other hand, those normal to the shoreline can be hardly determined from the previous field observations with the electromagnetic currentmeters. In the present analysis by means of the empirical eigenfunctions, however, the positions of nodal lines normal to the shoreline are easily determined by drawing strait lines normal to the shoreline passing the points of zero crossings of the empirical eigenfunctions in Fig. 13. For the points of zero crossings of the eigenfunctions correspond to the nodes of the standing edge waves at the shoreline. Figure 18 shows the nodal lines for n=1 to 6 mode, which are obtained in the way described above. In this figure, the positions of the wave staffs (black circle 1~4, 6~9) and the electromagnetic currentmeters (open circle A~C) are also plotted.

4.4 Cross-spectral analyses of current velosities in the surf zone

In order to confirm the existence of the standing edge waves which is cleared by the analysis of the empirical eigenfunctions, the cross-spectral analyses have been done for the offshore and the longshore components of the current velosities at the points A, B and C. A sampling interval of data is Δt=1 second and a number of data is N=4096 (about 68 minutes). The equivalent degree of freedom with a filter used for smoothing is r=16.

(1) Relation between U and V at the point C

Figure 19 shows the result of cross-spectral analysis between the velocity components of the offshore (U_c) and the longshore (V_c) directions at the point C. The arrows in Fig. 19 denote the frequencies of the standing edge waves of cut-off modes which are obtained by means of the empirical eigenfunctions (see Table 5). Both the spectral peaks and the coherences of U_c versus V_c are recognized to be high at the frequencies denoted by the arrows with n= 1,4,5 and 6. At the frequency indicated by n=2, however, the coherence is too low in spite of the energy density of U_c being high enough. And at the frequency indicated by n=3, the spectral peaks are not sufficiently recognized and the coherence is very low.

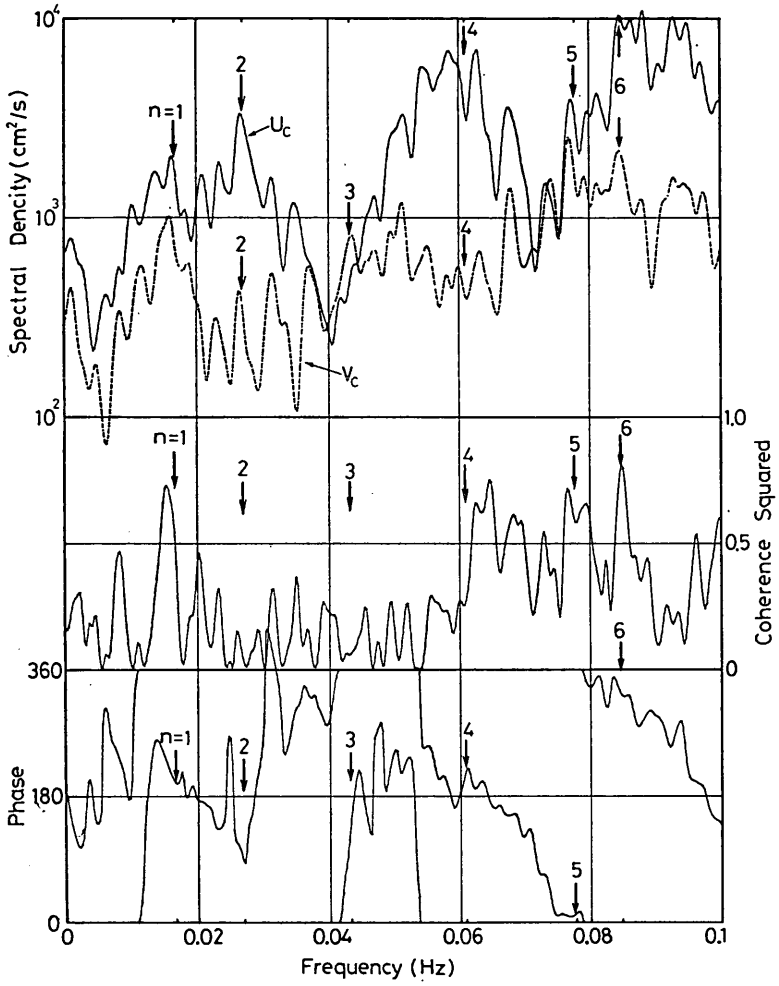

Fig. 19 Spectral densities, coherence and phase difference between offshore and longshore components of current velocity at point C

These features of the result of cross-spectral analysis have to be examined by taking into consideration the relative positions of the point C and the nodal lines of the standing edge waves which are shown for n=1~6 modes in **Fig. 19**, and also by taking into consideration the phase relationship between the two components of velocity which is shown for n=2 mode in **Fig. 4**.

According to **Fig. 18**, the point C was located near the nodal line of the standing edge wave of n=1 mode, but it was apart from both the points of intersection of the nodal lines and antinodes in the sence of the three dimensions. Because of this, **Fig. 19** indicates that there exist the peaks of energy densities of the two velocity components and the coherence between these components is high at the frequency corresponding to n=1 mode. As can be

easily predicted from Fig. 18, the phase difference between the two components of current velocity is 180 degrees for $n=1$ mode at the point C. This feature is confirmed in Fig. 19, since the phase difference is nearly equal to 180 degrees at the frequency indicated by $n=1$.

For the standing edge wave of $n=2$ mode, the point C was located at the antinode in the sense of the three dimensions as shown in Fig. 18. This means that both the offshore and the longshore components of current velocity due to the standing edge waves of $n=2$ mode become zero as seen in Fig. 4. Therefore, the coherence should not be high and the phase relationship should not be in phase at the frequency indicated by $n=2$. The low coherence and the unmatched phase relationship at this frequency are materialized as demonstrated in Fig. 19, though the spectral density of U_c holds a relatively high value.

For the standing edge wave of $n=3$ mode, point C was located at the point of intersection on the modal lines, where both the offshore and the longshore components of current velocity due to this wave are also equal to zero as can be easily supposed from Fig. 4. Therefore, the energy densities of both the components of current velocity should be low, the coherence low and the phase relationship not in phase. These are confirmed at the frequency indicated by $n=3$ in Fig. 19.

For the standing edge wave of $n=4$ mode, the point C was located apart from both the points of intersection of the nodal lines and the antinodes. Because of this, at the frequency a little higher than that indicated by $n=4$ in Fig. 19, the coherence is high and the phase difference is almost equal to 180 degrees. The energy density of U_c is, however, unexpectedly higher than that of V_c. The location of the point C is not near the nodal line parallel to the shoreline but near that normal to the shoreline. At this relative position, the longshore component of current velocity (V_c) is expected to be greater than the offshore one. The reasons for this contradiction are not known. The accuracy of drawing the nodal line normal to the shoreline might not be so good, because the point of the node at the shoreline is not so clear for the eigenfunction of e_4 in Fig. 13.

For the standing edge waves of $n=5$ and 6 modes, the point C was located near the point of intersection of nodal lines (for $n=5$) and the antinode (for $n=6$), respectively. Under these conditions, the coherences should not be essentially high in the same reason as for $n=2$ and 3. The high coherences, however, are recognized at the frequencies indicated by $n=5$ and 6 in Fig. 19. Moreover, the peaks of energy densities exist and the phase relationships are almost in phase at these frequencies. These contradictions can be explained as follows. Almost all energy of the edge wave concentrates inside the area with the distance equivalent of about one longshore wavelength of the edge

wave from the shoreline. This area gradually becomes narrower with the increase of the modal number of the edge wave. Therefore, the edge wave of higher mode is affected more significantly by the sea bottom topography with the longshore bar. Because of this, the error due to the approximation of the beach profile by Eq. (40) becomes to be noticeable with the increase of the modal number, and as a necessary consequence the positions of the nodal lines parallel to the shoreline determined by using Eq. (22) might have differed from the actual ones.

Thus, the features of **Fig. 19** are well explained by the theory of the standing edge waves. But the phase difference continuously decreases with the frequency higher than 0.06Hz. The same tendency was noticed in the results of cross-spectral analyses by Huntley & Bowen[4]. The cause of this

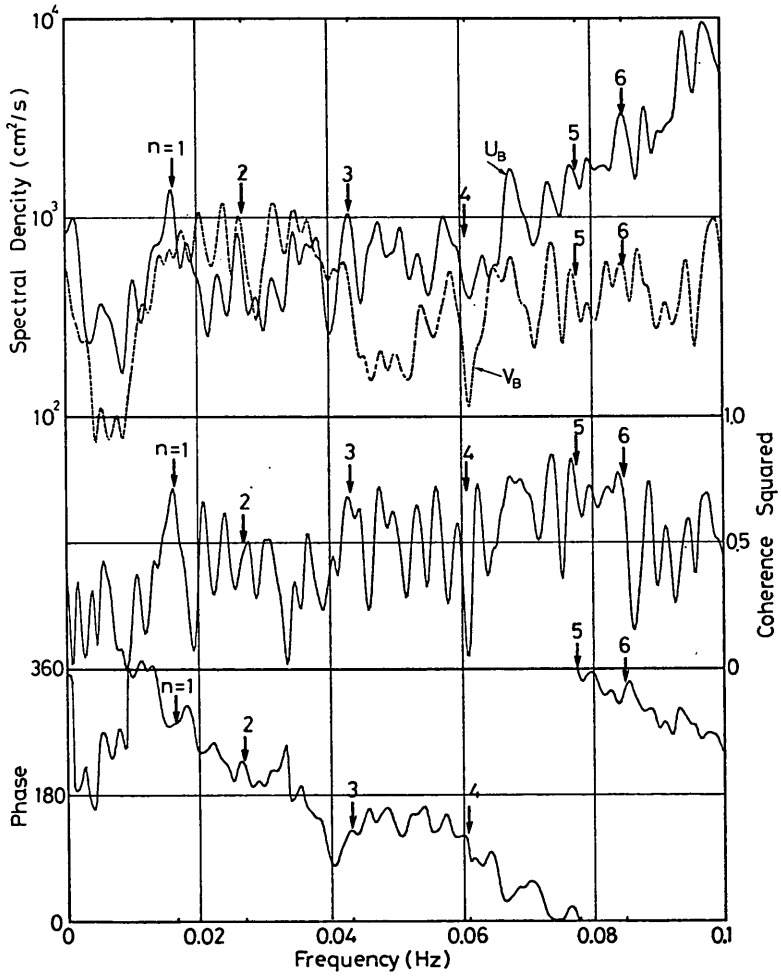

Fig. 20 Spectral densities, coherence and phase difference between offshore and longshore components of current velocity at point B

phenomenon is still unexplained.

(2) **Relation between U and V at the point B**

Figure 20 shows the result of cross-spectral analysis between the offshore (U_B) and the longshore (V_B) components of the current velocity at the point B. At the frequency described by $n=1$, the energy densities are large and the coherence is high, but the phase relationship is not in phase. At the frequency for larger modes than this, there is nothing to be explained clearly.

According to the whole current pattern in the investigated area which is shown in **Fig. 12**, the longshore current changes its direction to the offshore direction near the point B. In the physical sense, the point B is located inside the zone of currents similar with rip feeder currents, where the magnitude relationships of two components of current velocity usually differ from those predicted by the theory of the edge waves as pointed out by Chappell & Wright[23]. Because of this, it is considered that the phenomena due to the standing edge waves do not sufficiently appear in the cross-spectral analysis. Also in this case, the phase difference continuously decreases with the frequency higher than 0.01Hz.

(3) **Relation between the offshore velocities of the points B and C**

Figure 21 shows the result of cross-spectral analysis between the offshore components of current velocities at the points B (U_B) and C (U_C). At the frequency of every modal number except $n=3$, the coherence is clearly high and the phase difference is almost zero degree. According to **Fig. 18**, both tho points B and C were located near the positions of intersections of nodal lines for the standing edge wave of $n=3$ mode. Then, the coherence at the frequency described by $n=3$ is not high. At another frequency denoted by an arrow with a asterisk (*), the energy densities of both the offshore components of current velocities are large and the coherence is high. This is, however, considered to be due to the incoming waves since the phase relationship differs from that of the standing edge wave.

Since the point A was located near the rather complicated boundary with the wing breakwater, the standing edge waves are not noticed clearly in the result of cross-spectral analysis between two components of current velocity at this point.

(4) **Relation between surface fluctuations**

According to **Fig. 18**, the wave staffs of No. 1 to No. 4 were located approximately along the nodal line parallel to the shoreline for every odd mode. All the staffs were located along or near the nodal lines for $n=4$ to 6 modes. Those of No. 6, No. 7 and No. 9 were located approximately along the nodal line and those of No. 3, No. 4, No. 8 and No. 9 were located near the nodal line for $n=2$ mode. That is to say, the many staffs were unfortunately located along or near the nodal lines of every mode. Under these conditions, the

peaks of spectral densities of surface fluctuations due to the standing edge waves hardly appear in the spectra of waves at these points. And the data of surface fluctuations read from the 16mm films contain some errors due to the several reasons as previously mentioned. Because of this, the enough results to indicate the existence of the standing edge waves have not been obtained through the cross-spectral analyses of pairs of these wave data.

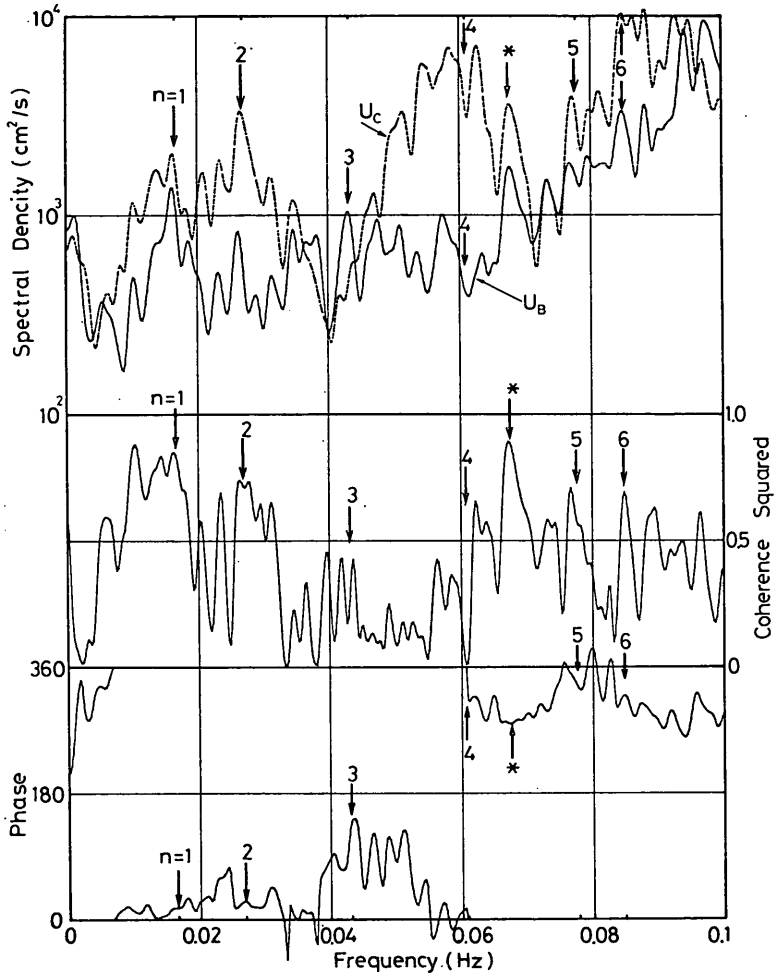

Fig. 21 Spectral densities, coherence and phase difference between offshore components of current velocities at points B and C

4.5 Some features related to standing edge waves

In the investigated area, there was the longshore current with the large clockwise circulation as shown in **Fig. 12**. This longshore current was too strong to form the rhythmic topographies such as the cresentic bars in the sea bed and the cusps on the foreshore as pointed out by Huntley & Bowen[12]. But the longshore bar was formed in parallel with the shoreline about 50

meters offshore from the shoreline as shown in Fig. 7. As seen in Fig. 2, the node of the standing edge wave of every odd mode and the antinode of every even mode concentrate in this place.

Bowen & Inman[2] suggest that the rip currents will occur at the antinodes of the standing edge wave. No rip current was detected by tracking the floats in the investigated area. But the author visually confirmed it at the slightly right hand side of the reference point No. 29, where the phase of the standing edge wave of $n=1$ mode will become that of the antinode if the empirical eigenfunction of e_1 will be extrapolated in the longshore direction beyond the reference point No. 29.

Bowen & Inman[2] also suggest that the height of incoming waves becomes higher due to the interaction with the standing edge wave at the antinode of the later. The wave measurement point of No. 2 was located nearly at the antinode of the standing edge wave of $n=2$ mode as seen in Fig. 18. At this point, the rate of wave breaking was slightly larger than that of around. These may be items of evidence which support the idea of Bowen & Inman.

5. Conclusions

The field observation was carried out in order to detect the edge waves at Sendal Beach, Japan. The longshore variations of wave run-up fronts on the foreshore were read from the aerophotographs. And the waves and currents velocities in the surf zone were measured at the same time.

By analyzing the longshore variations of wave run-up fronts on the foreshore by means of the empirical eigenfunctions, the existence of the standing edge waves is demonstrated. The longshore wave numbers of these standing edge waves agree well with those of cut-off mode predicted by Ball's theory. Moreover, it is shown that the amplitude of the standing edge wave is inversely proportional to its wave number (or its frequency).

The positions of nodal lines of these standing edge waves are determined. Those parallel to the shoreline are determined by the offshore distance from the shoreline with which the hypergeometric function becomes to be zero, while those normal to the shoreline are determined by drawing the straight lines normal to the shoreline passing the points of zero-crossings of the empirical eigenfunctions.

The cross-spectral nanlyses are conducted for pairs of two components of current velocities measured simultaneously in the surf zone. In these cross-spectra, it is recognized that at the particular frequencies the energy densities are large, the coherence is high and the phase relationship is in phase. These frequencies correspond to those of the standing edge waves of cut-off modes which are predicted from Ball's theory by using the longshore wavelengths of the empirical eigenfunctions. But there exist the standing edge waves of

particular modes at the frequencies of which these important features are not clearly recognized in the cross-spectra. In these cases, the measurement points are located at, or near, the point of intersections of the nodal lines or the antinodes of the standing edge waves of particular modes.

Acknowledgements

The author is grateful to Mr. Norio Tanaka, the Chief of the Littoral Drift Laboratory, for his encouragement and support for the present study as well as his critical reading of the manuscript and to Dr. Yoshimi Goda, the Director of the Hydraulic Engineering Division, for helpful suggestions and observation and his critical reading of the manuscript. In the field observation the author received kind assistances and advices from the following people: Mr. Kazuo Nadaoka, Mr. Hideo Osanai, Mr. Takamichi Kondo, Mr. Masahiro Akaishi (Member of the Littoral Drift Laboratory) and Mr. Eiji Tomida (Member of the Breakwaters Laboratory). The author is indebted to the Nearshore Environment Research Center for providing the 16 mm motion-picture cameras and the electromagnetic currentmeters. The author also should like to express his grateful thanks to the Siogama Port Construction Office and the Yokohama Investigation and Design Office, the Second District Construction Bureau, for their kind assistances. (Received June 29,1981)

References

1) Gallagher, B: Generation of surf beat by nonlinear wave interactions, J.F.M., Vol. 49, part 1, pp. 1-20, 1971.
2) Bowen, A.J. and D.L. Inman: Rip currents, 2 Laboratory and field observation, J.G.R., Vol. 74, No. 23, pp. 5479-5490, 1969.
3) Bowen, A.J. and D.L. Inman: Edge waves and crescentic bars, J.G.R., Vol. 76, No. 36, pp. 8862-8871, 1971.
4) Huntley, D.A. and A.J. Bowen: Beach cusps and edge waves, Proc. 14th Coastal Eng. Conf., pp. 1378-1393, 1978.
5) Lamb, H.: Hydrodynamics, 6th ed., Cambridge Univ. Press, Art. 260, 738p., 1932.
6) Ursell, F.: Edge waves on a sloping beach, Proc. Royal Society of London, Series A, Vol. 214, pp. 79-97, 1952.
7) Ball, F.K.: Edge waves in an ocean of finite depth, Deep-Sea Res., Vol. 14, pp. 79-88, 1967.
8) Guza, R.T. and A.J. Bowen: Finite amplitude edge waves, J. Mar. Res., Vol. 34, pp. 269-293, 1976.
9) Suhayda, J.N.: Standing waves on beaches, J.G.R., Vol. 79, No. 21, pp. 3065-3071, 1974.

10) Winant, C.D., D.L. Inman and C.E. Nordstrom: Discription of seasonal beach change using empirical eigenfunction, J.G.R., Vol. 80, No. 15, pp. 1979–1986, 1975.
11) Aubrey, D.G.: Seasonal patterns of onshore/offshore sediment movement, J.G.R., Vol. 84, No. C10, pp. 6347–6354, 1979.
12) Huntley, D.A. and A.J. Bowen: Field observation of edge waves, Nature, Vol. 243, No. 5403, pp. 160–162, 1973.
13) Huntley, D.A.: Long-period waves on a natural beach, J.G.R., Vol. 81, No. 36, pp. 6441–6449, 1976.
14) Sasaki, T. and K. Horikawa: Observation of nearshore current and edge waves, Proc. 16th Coastal Eng. Conf., pp. 791–809, 1978.
15) Holeman, R.A., D.A. Huntley and A.J. Bowen: Infragravity waves in storm conditions, Proc. 16th Coastal Eng. Conf., pp. 268–284, 1978.
16) Guza, R.T. and D.L. Inman: Edge waves and beach cusps, J.G.R., Vol. 80, No. 21, pp. 2997–3012, 1975.
17) Tanaka, N.: Beach erosion at the up-drift coast of a breakwater prolonged obliquely from the shore; Sendai Port, Coastal Sediments '77, 5th Symp. of the Waterway, Port, Coastal and Ocean Division of ASCE, pp. 1026–1041, 1977.
18) Katoh, K. et al.: Observation of hydraulic phenomena in the surf zone at the Sendai Beach (in September 1979), Technical note of Port and Harbour Research Institute, Ministry of Transport, Japan, No. 355, 30p., 1980. (in Japanese)
19) Nagata, Y.: The statistical properties of orbital wave motions and their application for the measurement of directional wave spectra, Journal of Oceanographical Society of Japan, Vol. 19, No. 4, pp. 169–181, 1964.
20) Holman, R.A. and A.J. Bowen: Edge waves on complex beach profiles, J.G.R., Vol. 84, No. C10, pp. 6339–6346, 1979.
21) Tanaka, N. and K. Katoh: On characteristics of longshore bars near the Agano River, Coastal Eng. in Japan, Vol. 23, pp. 274–278, 1976. (in Japanese)
22) Tanimoto, K., S. Haranaka, E. Tomida, Y. Izumida and S. Suzumura: A hydraulic experimental study on curved slit caisson breakwater, Report of Port and Harbour Research Institute, Ministry of Transport, Japan, Vol. 19, No. 4, pp. 3–53, 1980. (in Japanese)
23) Chappell, J. and L.D. Wright: Surf zone resonance and coupled mophology, Proc. 16th Coastal Eng. Conf., pp. 1359–1377, 1978.